Modeling of thermophysical properties in heterogeneous periodic media according to a multi- scale approach: Effective conductivity tensor and edge effects

A. Matine, Nicolas Boyard, Patrice Cartraud, Grégory Legrain, Y. Jarny

Modeling of thermophysical properties in heterogeneous periodic media according to a multi-scale approach: Effective conductivity tensor and edge effects

A. Matine [a], N. Boyard [a,*], P. Cartraud [b], G. Legrain [b], Y. Jarny [a]

[a] Université de Nantes, Nantes Atlantique Universités, Laboratoire de Thermocinétique de Nantes, UMR CNRS 6607, La Chantrerie, rue Christian Pauc, BP 50609, 44306 Nantes cedex 3, France
[b] Institut de Recherche en Génie civil et Mécanique (GeM), UMR CNRS 6183 Ecole Centrale de Nantes, BP 92101, 44321 Nantes cedex 3, France

The homogenization theory is a powerful approach to determine the effective thermal conductivity ten- sor of heterogeneous materials such as composites, including thermoset matrix and fibers. Once the effect ive properties are calculated, they can be used to solve a heat conduction problem on the composite structure at the macroscop ic scale. This approach leads to good approximations of both the heat flux and temperat ure fields in the interior zone of the structure; however edge effects occur in the vicinity of the domain boundaries. In this paper, following an approach proposed for elasticity problems, it is shown how these edge effects can be accounted for. An additional asymptotic expansion term is introduced, which plays the role of a ''heat conduction boundary layer'' (HCBL) term. This expansion decreases expo- nentially and tends to zero far from the boundary. Moreover, the HCBL length can be determined from the solution of an eigenvalues problem. Numerical examples are considered for a standard multilayered material and for a unidirection al carbon-epoxy composite. The homogenized solutions computed with a finite element software, and corrected with the HCBL terms are compared to a heterogeneous finite ele- ment solution at the microscopic scale. The influences of the thermal contrast and the scale factor are illustratedfordifferentkindof boundaryconditions.

1. Introduction

Composite materials represent an innovative technological solution to improve and create more competitive products in many industrial sectors. In leading-edge domains such as aeronautics, the high performances of composites are an undeniable asset. Metals are then gradually substituted by composites in airplane structures. However, even if it has great advantages for mechanical issues, it may lead to some drawbacks regarding heat transfer. Composite materials are heterogeneous media actually so insulating compared to metallic ones that heat confinement issues rapidly occur. To predict the thermal environment of airplane structures (and the associated thermo-mechanical behavior) for design purpose, thermal properties and the associated uncertainties of involved orthotropic composite structures are thus required.

Reliable and efficient methods are necessary for their characterization. They have to take into account one of the main features of such structures: the multiple spatial scales involved in the heat conduction process. Two parallel distinct and complementary approaches can be considered for this issue. The first one is experimental and consists in using dedicated devices to measure, at the macroscopic level, the effective anisotropic thermal properties of samples, by using the classical transient flash [1] or hot wire [2] methods, or a specific hot disc method [3]. Measurements can also be done at the microscopic level to characterize each component of the structure, with a spatial resolution of a few cubic micrometers [4]. The second is a multi-scale approach and aims to calculate the effective thermal conductivity tensor from data known at the scale of the components. Volume averaging methods have been widely developed to specify the relationships between the microstructure, the component properties and the corresponding macroscopic parameters [5–7]. Most of these works have been developed for modeling heat transfer and/or fluid flow within porous materials. With the same goal, periodic homogenization based on the asymptotic expansion method has been also very fruitful [7–12]. This method was also developed for modeling porous material [12], but in this paper we only consider heat conduction in periodic structures without advection term. Then, no transport term will appear in the homogenized equations, and no contact between fluid and solid phases has to be modeled. Thanks to this approach, the initial heat conduction problem posed on the heterogeneous

* Corresponding author. Tel.: +33 (0)2 40 68 31 11; fax: +33 (0)2 40 68 31 41.
E-mail address: nicolas.boyard@univ-nantes.fr (N. Boyard).

Nomenclature

Latin letters

e_i	Space vectors
d_m	Depth of the (HCBL) heat conduction boundary layer
f	Volume heat source
G_m	Semi-infinite domain
$\widetilde{G}_m$	Truncated semi-infinite domain
h, h^*	Heat transfer coefficient, modified heat transfer coefficient
k_{ij}	Heat conductivity component
$\boldsymbol{K}$	Heterogeneous thermal conductivity tensor
$\boldsymbol{K}^*$	effective heat conductivity tensor
L_i	Sizes of the 3-D parallelepiped domain
l_i	Sizes of the periodic cell
$\boldsymbol{n}$	Outward unit normal
R_{hom} R_{het} R_{const}	Thermal resistances of the homogeneous wall. the heterogeneous wall, thermal constriction
$T_{BL}^{1,m}$	Temperature correcting term at the order $k=1$, associated to the boundary Γ_m
T^{ϵ}	Heterogeneous temperature field
T^k	homogenized approximation of T^{ϵ} at the order k
T_{ext}	External temperature
$\boldsymbol{Y}$	spatial domain of the periodic cell
$\boldsymbol{x}$, $\boldsymbol{y}$, $\boldsymbol{s}$	Space variables

Greek letters

$\partial\Omega$, ∂Y	Boundary of Ω, of the cell Y
δ_m	Scalar solution of the eigenvalues problems
ε	Scale factor
Γ_i	Boundaries of Ω
φ_i	Normal outward component of the heat flux on the boundary
$\boldsymbol{\varphi}^0$	Homogenized heat flux, at the order 0
$\boldsymbol{\varphi}^{\epsilon}$	Heterogeneous heat flux field
$\boldsymbol{\phi}_{\boldsymbol{BL}}^{\boldsymbol{0,m}}$	Heat flux correcting term at the order $k=0$, associated to the boundary Γ_m
κ	Thermal contrast
$\boldsymbol{\Psi}_{\boldsymbol{i}}^{\boldsymbol{m}}$	Solution of the eigenvalues problems
χ_i^m	Solutions of elementary problems, on $\widetilde{G}_m$
τ_f	Volume fiber ratio
$w_i(\boldsymbol{y})$	Solutions of elementary problems, on $\boldsymbol{Y}$
Ω	Spatial domain of the piece

domain is split in two problems. One is solved on the periodic cell at the microscopic scale: this solution provides the effective thermal properties of the medium. The second is a macroscopic problem, whose solution enables the determination of homogenized temperature and heat flux fields in the part. Asymptotic expansion method applied to heat conduction problem is not straightforward since the homogenized problems depend on several parameters such as thermal contact between components or thermal conductivity contrast with respect to scale ratio [12]. The same approach was developed for non periodic structures, but it requires the determination of the representative volume element as in random structures [13,27] for example. This approach leads to good approximations of both the heat flux and temperature in the interior zone of the structure, as long as the periodicity is satisfied.

However edge effects occur in the vicinity of the domain boundaries due to the loss of periodicity. These edge effects are well known in thermal science and are of crucial importance for all heat conduction modeling, especially at the interface between different media [14]. They are sometimes analyzed as thermal constriction effect [15,16]. It is thus mandatory to take them into account, within the framework of the asymptotic expansion method, as it has been done in numerous works in mechanics [17–20] see also the references cited in the review papers [21,22]. The different approaches which have been proposed may be classified into three categories. In the first one, another expansion corresponding to boundary layers is considered [17–19]. It can be shown that the boundary layer solution decay rapidly with respect to the distance from the edge. This originates another class of method, for which the objective is to define boundary conditions for the homogenized problem, such that a good approximation of the exact solution will be obtained in the interior zone of the domain [20]. A third category of method combines two models, a microscale model in the boundary layer domain, and a macroscale model outside this domain with appropriate interface conditions [23]. However, as far as we know, only few works have addressed edge effects for thermal applications, introducing the concepts of "heat conduction boundary layer" (HCBL) and constriction resistance [16]. Within this context, we thus focus on the study of such HCBL and edge effect problem in steady state in a first step, following the approach of H. Dumontet [19] for elasticity, based on the introduction of another expansion in the vicinity of the boundary. The study of edge effects can be extended for the homogenized transient problem [24]. More generally, several authors [14,25–28], have studied the question of modeling the boundary conditions of porous medium, including the contact between the solid and the fluid phases in the interfacial region. In case of a surface with periodic roughness, correcting terms of the temperature and heat flux fields can be also computed (see e.g. [29]). Such edge effects are out of the scope of this paper and will be not considered in the following.

The outline of the paper is as follows: in a first part, we first briefly recall the main homogenization results, based on the asymptotic expansion method and we present the correction of edge effects by introducing the "heat conduction boundary layer" terms, as the solution of a specific heat conduction problem at the micro-scale level. We consider only the heat conduction problem, without any transport term. Three kinds of boundary conditions are considered. It is shown how the size of the boundary layer can be determined by solving an eigenvalues problem.

In a second part, we compare the temperature and heat flux fields obtained from the numerical solution of the heterogeneous and the homogenized problems respectively. Two cases are studied: one is a multilayered structure; the other one is a unidirectional composite which involves parallel cylindrical fibers within an insulating polymer matrix. The influences of scale factor, thermal contrast and volume fraction are discussed.

2. Periodic homogenization

2.1. Problem statement – A multi-scale approach

Let us consider a piece of heterogeneous periodic material, Fig. 1, defined in a bounded domain $\Omega \subset R^3$. The macroscopic coordinates of a point of Ω are denoted $\boldsymbol{x}=[x_1,x_2,x_3,]$ in a Cartesian coordinate system $\{0,\boldsymbol{e}_1,\boldsymbol{e}_2,\boldsymbol{e}_3\}$

The boundary $\partial\Omega$ is subdivided in three distinct parts, $\partial\Omega=\bigcup_{i=1}^{3}\Gamma_i$, in order to consider three different usual kinds of boundary conditions associated to the heat conduction problem:

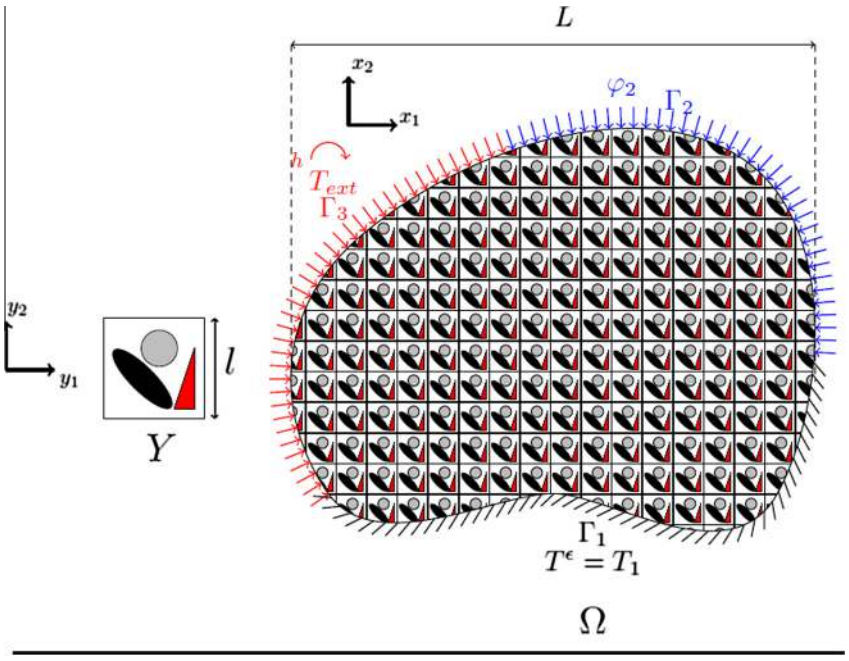

Fig. 1. The spatial domain Ω of the heterogeneous periodic medium and the associated periodic cell Y.

- A Dirichlet condition on Γ_1 where the temperature is fixed to T_1(constant for simplicity), this value will be taken equal to zero without loss of generality
- A Neumann condition on Γ_2 where the normal outward component of the heat flux is fixed by (a varying function) $\varphi_2(s)$, $s \in \Gamma_2$,
- A Fourier condition on Γ_3 where the normal outward component of the heat flux $\varphi_3(s) = h[T(s) - T_{ext}(s)]$, is fixed by an external temperature $T_{ext}(s)$, $s \in \Gamma_3$ and a heat transfer coefficient h.

A spatially distributed (and stationary) volume heat source $f(\boldsymbol{x})$,$\boldsymbol{x} \in \Omega$ can be considered all over the spatial domain.

The heterogeneous fields are denoted respectively T^ϵ (temperature) and φ^ϵ (heat flux) in Ω. These fields satisfy the following set of steady heat conduction equations together with the three kinds of boundary equations

$$div_x(-\boldsymbol{\varphi}^\epsilon(\boldsymbol{x})) = f(\boldsymbol{x}) \quad \text{in } \Omega \tag{1a}$$
$$\boldsymbol{\varphi}^\epsilon(\boldsymbol{x}) = \boldsymbol{K}\nabla_{\boldsymbol{x}} T^\epsilon(\boldsymbol{x}) \quad \text{in } \Omega \tag{1b}$$
$$T^\epsilon(s) = T_1, \ s \in \Gamma_1 \ \text{(Dirichlet condition)} \tag{1c}$$
$$\boldsymbol{\varphi}^\epsilon(s) \cdot \boldsymbol{n} = \varphi_2 s \in \Gamma_2 \ \text{(Neumann condition)} \tag{1d}$$
$$\boldsymbol{\varphi}^\epsilon(s) \cdot \boldsymbol{n} = h(T^\epsilon - T_{ext}) s \in \Gamma_3 \ \text{(Fourier condition)} \tag{1e}$$

where $\boldsymbol{n}$ is the outward unit normal and $\boldsymbol{K}$ the heterogeneous thermal conductivity tensor; it is cell-periodic and each component $k_{ij}(\boldsymbol{y})$; $i,j = 1,2,3$ depends on the local variable $\boldsymbol{y}$ (microscopic scale) in the cell domain $\boldsymbol{Y}$.

Instead, the heterogeneous material is assumed to have a periodic structure. The periodic cell (see the Fig. 1), is denoted $\boldsymbol{Y} = \prod_{i=1}^{3}[0, l_i]$, and $\boldsymbol{y} = (y_1, y_2, y_3) \in \boldsymbol{Y}$ are the coordinates of a cell point. The scale factor $\boldsymbol{\varepsilon}$ is the ratio between the size of $\boldsymbol{Y}$ and the size of Ω, the microscopic coordinates are thus defined from $\boldsymbol{y} = \varepsilon^{-1}x$.

2.2. Asymptotic expansion method

Assuming that the scale factor ε is small enough, the asymptotic expansion method is used [9,12], and the temperature T^ϵ can be developed under the following form:

$$T^\epsilon(\boldsymbol{x},\boldsymbol{y}) = T^0(\boldsymbol{x},\boldsymbol{y}) + T^1(\boldsymbol{x},\boldsymbol{y}) \cdot \epsilon + T^2(\boldsymbol{x},\boldsymbol{y}) \cdot \epsilon^2 + \cdots; \quad \boldsymbol{x} \in \Omega, \ \boldsymbol{y} \in \boldsymbol{Y} \tag{2}$$

where T^k is the approximation of T^ϵ at the order k, and is supposed to be periodic at the microscopic scale. Moreover it is assumed that the thermal conductivity of each components of the heterogeneous structure have the same order of magnitude, which means that the thermal contrast is not too large. In practice, this is the case for most of composites used in aeronautic.

It can be classically shown [12] that:

- The first term T^0 depends only on the macroscopic variable $\boldsymbol{x}$, and is the solution of an homogenized heat conduction problem in the domain Ω with an effective heat conductivity tensor $\boldsymbol{K}^*$:

$$\text{div}_x(-\langle\boldsymbol{\varphi}^0\rangle(x)) = f(x) \quad \text{in } \Omega \tag{3.a}$$
$$T^0(s) = T_1 \quad \text{on } \Gamma_1 \tag{3.b}$$
$$\langle\boldsymbol{\varphi}^0\rangle \cdot \boldsymbol{n} = \varphi_2 \quad \text{on } \Gamma_2 \tag{3.c}$$
$$\langle\boldsymbol{\varphi}^0\rangle \cdot \boldsymbol{n} = h(T^0 - T_{ext}) \quad \text{on } \Gamma_3 \tag{3.d}$$
$$\text{Where } \langle\boldsymbol{\varphi}^0\rangle(x) = \boldsymbol{K}^* \cdot \nabla_{\boldsymbol{x}} T^0(x) \text{ in } \Omega \tag{3.e}$$
$$\text{and } \langle\cdot\rangle = \frac{1}{|Y|}\int_Y [\cdot] dY, \tag{3.f}$$

- The second term $T^1(x,\boldsymbol{y})$ can be written in the following form

$$T^1(\boldsymbol{x},\boldsymbol{y}) = \sum_{i=1}^{3} \frac{\partial T^0}{\partial x_i}(\boldsymbol{x}).w_i(\boldsymbol{y}) = (\nabla T^0(\boldsymbol{x}))^t \cdot \boldsymbol{w}(\boldsymbol{y}) \tag{4}$$

where the functions $w_i(\boldsymbol{y})$, $i = 1,2,3$, are solutions of the elementary problems, set on $\boldsymbol{Y}$

$$\begin{cases} \text{div}_y(\boldsymbol{K}(\boldsymbol{y})(\boldsymbol{e_i} - \nabla_{\boldsymbol{y}}\boldsymbol{w_i}(\boldsymbol{y}))) = 0; & (5.a) \\ \boldsymbol{w_i} \quad \text{periodic on } \partial\, Y & (5.b) \end{cases} \tag{5}$$

The terms of the homogenized tensor $\boldsymbol{K}^*$ are independent of the variable y, and are given by ($i, j = 1,\ldots,3$):

$$K^*_{i,j} = \frac{1}{|Y|}\int_Y [\boldsymbol{K}(\boldsymbol{y})(\boldsymbol{e_i} - \nabla_{\boldsymbol{y}} w_i(\boldsymbol{y}))]^t \boldsymbol{e_j} dY \tag{6}$$

- The heat flux, at the order 0, is given by:

$$\boldsymbol{\varphi}^0(\boldsymbol{x},\boldsymbol{y}) = (\boldsymbol{K}(\boldsymbol{y}).[\boldsymbol{e_i} - \nabla_{\boldsymbol{y}} w_i(\boldsymbol{y})]\boldsymbol{e_j})\nabla_{\boldsymbol{x}} \boldsymbol{T}^0(\boldsymbol{x}) \tag{7}$$

Periodic homogenization provides heat flux $\boldsymbol{\varphi}^0$ and temperature T^0 fields, which are good approximations of the heterogeneous solutions $\boldsymbol{\varphi}^\epsilon$ and T^ϵ far enough from the boundary $\partial\Omega = \bigcup_{i=1}^{3}\Gamma_i$ of the domain. However, this approximation is not satisfactory anymore close to the boundary. This is first due to the loss of periodicity. The second reason is that $\boldsymbol{\varphi}^0$ is generally not compatible with an arbitrary Neumann or Fourier conditions, since these conditions are only satisfied in a weak sense (see Eqs. 3.c,3.d and 3.e).

We can thus underline that the classical theory of homogenization of periodic media provides a rather bad description of the heterogeneous fields close to the boundary. Consequently, it is necessary to improve the accuracy of the homogenized solutions (temperature and/or heat flux) in the vicinity of the boundary. Correcting terms of edge effects have thus to be determined.

2.3. Correction of the edge effects

The method developed in this work has been first proposed for elasticity problems by Dumontet [19]: it consists in introducing additional terms in the asymptotic expansion of the homogenized solution, which have an effect essentially in the vicinity of the boundaries. It is shown in the following how the determination of these additional terms depends on the kind of the boundary conditions.

For sake of simplicity and clarity, the spatial domain will be considered as a rectangular parallelepiped $\Omega = \prod_{i=1}^{3}[0, L_i]$, and only two elementary cases will be studied separately: one to determine the correcting terms associated to the Neumann condition (Fig. 2a) and one to the Fourier condition (Fig. 2b).

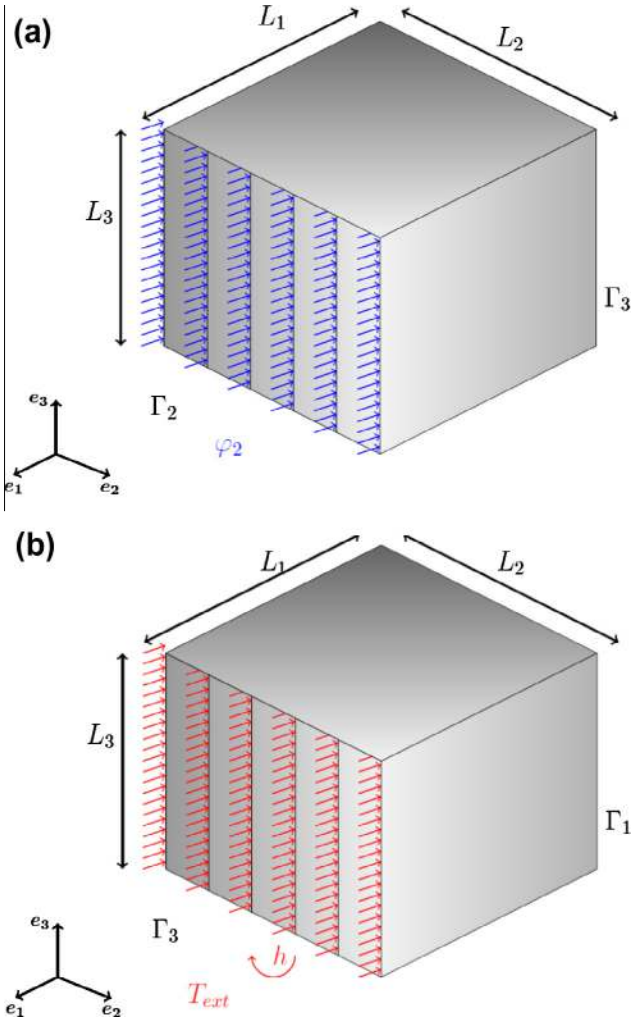

Fig. 2. The 3-D spatial domain Ω and its boundary conditions: (a) – Neumann & Dirichlet boundary conditions; (b) – Fourier and Dirichlet boundary conditions.

Each of these conditions will be fixed uniform only on the left face, named Γ_2 or Γ_3 at ($x_1 = 0$) of the parallelepiped, together with a Dirichlet condition on the opposite face, at $x_1 = L_1$, named Γ_1. To avoid the computation of correcting terms due to effects of the other edges and corner effects, conditions of periodicity will be considered on the four other faces of the parallelepiped. However, the method is quite general and can be applied to more complex situations.

The asymptotic expansion of the temperature is now written as follows.

$$T^\epsilon(\boldsymbol{x},\boldsymbol{y}) = T^0(\boldsymbol{x}) + (T^1(\boldsymbol{x},\boldsymbol{y}) + T^1_{BL}(\boldsymbol{x},\boldsymbol{y})) + \cdots, \quad \boldsymbol{x}\in\Omega,\ \boldsymbol{y}\in\boldsymbol{Y} \tag{8a}$$

$$T^1_{BL}(\boldsymbol{x},\boldsymbol{y}) = \sum_{\boldsymbol{m}=1}^{3} T^{1,m}_{BL}(\boldsymbol{x},\boldsymbol{y}) \tag{8b}$$

and the additional term T^1_{BL} results of the superposition of elementary terms $T^{1,m}_{BL}(\boldsymbol{x},\boldsymbol{y})$ which are depending on the kind of boundary conditions on Γ_m,$m = 1$, 2 or 3

2.3.1. Correcting terms associated to a Neumann or a Fourier condition, m = 2 or 3

It is shown in Appendix A, how the correcting terms associated to each of these conditions are determined. The approaches are similar, however, in the next Section 3, the numerical examples will illustrate the difference. To define $T^{1,m}_{BL}$, a semi-infinite domain (Fig. 3) is considered in the direction $\boldsymbol{e}_1$ normal to the face Γ_m, and denoted by

$$G_m =]0,\infty[\times]0,l_2[\times]0,l_3[, \quad m = 2,3 \tag{9.a}$$

The surface of G_m at ($x_1 = 0$) is denoted Γ'_m, and $\Gamma'_m \subset \Gamma_m$. The term $\boldsymbol{T}^{1,\boldsymbol{m}}_{\boldsymbol{BL}}$ is thus defined for $\boldsymbol{x}\in\Gamma_m$ and $\boldsymbol{y} = (y_1,y_2,y_3)\in G_m$, it is periodic in the $\{\boldsymbol{e}_2,\boldsymbol{e}_3\}$ directions. In practice for the computation of the correcting terms, the semi-infinite domain will be truncated in the $\boldsymbol{e}_1$ direction:

$$\widetilde{G}_m =]0,d_m[\times]0,l_2[\times]0,l_3[, \quad \text{with } d_m \leqslant L_1 \tag{9.b}$$

By introducing the set of functions $\chi^m_i(\boldsymbol{y})$, $i = 1,2,3$; $m = 2$ or 3 , solutions of the following elementary problems, on the sub-domain G_m:

$$\mathrm{div}_y(\boldsymbol{K}(\boldsymbol{y})(\nabla_y\chi^m_i(\boldsymbol{y}))) = 0 \ \text{ in } G_m \tag{10.a}$$

$$\boldsymbol{K}(\boldsymbol{y})(\nabla_y\chi^m_i(\boldsymbol{y}))\cdot\boldsymbol{n} = -\boldsymbol{K}(\boldsymbol{y})((\boldsymbol{e_i}+\nabla_y w_i(\boldsymbol{y})))\cdot\boldsymbol{n} + \frac{1}{|Y|}\int_{\boldsymbol{Y}}\boldsymbol{K}(\boldsymbol{y})(\boldsymbol{e_i}+\nabla_y\boldsymbol{w_i}(\boldsymbol{y}))\boldsymbol{d}Y\cdot\boldsymbol{n} \ \text{ on } \Gamma'_m \tag{10.b}$$

$$\chi^m_i(\boldsymbol{y}) \ \text{ periodic along the } \{\boldsymbol{e}_2,\boldsymbol{e}_3\} \text{ directions} \tag{10.c}$$

$T^{1,m}_{BL}(\boldsymbol{x},\boldsymbol{y})$ can be put under the following form (details are given in Appendix A):

$$T^{1,m}_{BL}(\boldsymbol{x},\boldsymbol{y}) = \sum_{i=1}^{3}\frac{\partial T^0}{\partial x_i}(\boldsymbol{x})\chi^m_i(\boldsymbol{y}) = (\chi^m(\boldsymbol{y}))^t\nabla_{\boldsymbol{x}}\boldsymbol{T}^0(\boldsymbol{x}) \tag{11}$$

While the correcting term of the heat flux is given by:

$$\boldsymbol{\phi}^{0,\boldsymbol{m}}_{\boldsymbol{BL}}(\boldsymbol{x},\boldsymbol{y}) = \boldsymbol{K}(\boldsymbol{y})(\nabla_y\boldsymbol{\chi}^m(y)).\nabla_x\boldsymbol{T}^0(\boldsymbol{x}) \tag{12}$$

2.3.2. Correcting terms associated to a Dirichlet condition on the opposite face Γ_1

A similar approach (see Appendix A) can be considered to determine the additional term $T^{1,1}_{BL}(\boldsymbol{x},\boldsymbol{y})$, in the vicinity of the boundary Γ_1, on a semi-infinite sub-domain:

$$G_1 =]-\infty,L_1[\times]0,l_2[\times]0,l_3[\tag{13}$$

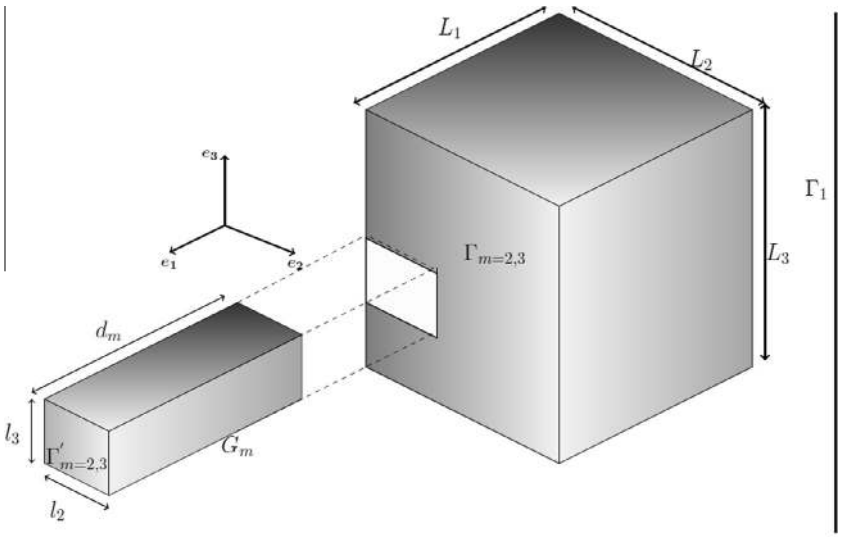

Fig. 3. The semi-infinite domain G_m associated to a Neumann or a Fourier condition.

It leads to the following results, for $\boldsymbol{x} \in \Gamma_1$ and $\boldsymbol{y} = (y_1, y_2, y_3) \in G_1$

$$T^{1,1}_{BL}(\boldsymbol{x},\boldsymbol{y}) = \sum_{i=1}^{3} \frac{\partial T^0}{\partial x_i}(\boldsymbol{x}).\chi^1_i(\boldsymbol{y}) \tag{14}$$

With the functions $\chi^1_i(y),\ i = 1,2,3$, solutions of the following elementary problems, on the sub-domain G_1:

$$\nabla_y(\boldsymbol{K}(\boldsymbol{y})(\nabla_{\boldsymbol{y}}\chi^1_i(\boldsymbol{y}))) = 0 \quad \text{in } G_1 \tag{15.a}$$

$$\chi^1_i(\boldsymbol{y}) = -w_i(\boldsymbol{y}) \quad \text{on } \Gamma'_1 \tag{15.b}$$

$$\chi^1_i(\boldsymbol{y}) \quad \text{periodic along the } \{\boldsymbol{e_2}, \boldsymbol{e_3}\} \quad \text{directions} \tag{15.c}$$

In practice for the computation of the correcting terms, the semi-infinite domain G_1 will be truncated in the $\boldsymbol{e}_1$ direction to

$$\widetilde{G}_1 =]L_1 - d_1, L_1[\times]0, l_2[\times]0, l_3[, \quad \text{with } d_1 \leqslant L_1 \tag{16}$$

2.3.3. Homogenized solutions with correcting terms of edge effects for both cases

Finally, in both cases considered above, the correcting terms $T^1_{BL}(\boldsymbol{x},\boldsymbol{y})$ associated to the Neumann & Dirichlet boundary conditions (case 1), or to the Fourier & Dirichlet boundary conditions (case 2), respectively on $\boldsymbol{\Gamma}_2$ and Γ_1, or $\boldsymbol{\Gamma}_3$ and Γ_1, takes the form:

$$T^1_{BL}(\boldsymbol{x},\boldsymbol{y}) = T^{1,1}_{BL}(\boldsymbol{x},\boldsymbol{y}) + T^{1,m}_{BL}(\boldsymbol{x},\boldsymbol{y}), \quad m = 2 \quad \text{or } 3 \tag{17}$$

In both cases, the homogenized solutions (temperature and heat flux), given by the asymptotic expansion truncated at the first order, and corrected by the boundary layer terms in the vicinity of these boundaries can be written in the matrix form:

$$T^{\epsilon}(\boldsymbol{x},\boldsymbol{y}) \approx T^0(\boldsymbol{x}) + [\boldsymbol{w}(\boldsymbol{y}) + \boldsymbol{\chi}^1(\boldsymbol{y}) + \chi^m(\boldsymbol{y})]^t \nabla_x \boldsymbol{T}^0(\boldsymbol{x}) \tag{18}$$

$$\phi^{\epsilon}(\boldsymbol{x},\boldsymbol{y}) \approx (\boldsymbol{K}(\boldsymbol{y}) \cdot [\boldsymbol{e} - \nabla_{\boldsymbol{y}}\boldsymbol{w}(\boldsymbol{y}) + \nabla_{\boldsymbol{y}}\chi^1(\boldsymbol{y}) + \nabla_{\boldsymbol{y}}\chi^m(\boldsymbol{y})]\boldsymbol{e})\nabla_{\boldsymbol{x}}\boldsymbol{T}^0(\boldsymbol{x}) \tag{19}$$

These results will be illustrated in Section 3 by two numerical examples. The homogenized solutions are compared to those of the heterogeneous problem. As already stated, the semi-infinite domains have to be truncated in practice. This point is developed in the following sub-section.

2.4. Determination of the boundary layer sizes- Truncation of the sub-domains G_j

For the determination of the functions $\boldsymbol{\chi}^j_i(\boldsymbol{y}),\ i = 1,2,3;\ j = 1,2,3$, the equations have been set on the semi-infinite domains $G_j,\ j \in \{1, m\}$; $m = 2$ or 3. It can be shown [30] that the correcting terms $T^{1,j}_{BL}(x,y)$ are decreasing exponentially when $y1$ tends to ± infinity. This property leads to express $\chi^j_i(\boldsymbol{y})$ in the following forms:

$$\chi^1_i(\boldsymbol{y}) = \Psi^1_i(\boldsymbol{y}).e^{-\delta_1(L_1 - y_1)} \tag{20.a}$$

$$\chi^j_i(\boldsymbol{y}) = \Psi^j_i(\boldsymbol{y}).e^{-\delta_j\ y_1}, \quad j = 2,3 \tag{20.b}$$

where the positive scalar terms δ_j have to be determined.

The functions $\chi^j_i(\boldsymbol{y})$ are computed on truncated sub-domains, Eq. (9.b) for the Dirichlet condition and Eq. (16) for the Neumann or the Fourier condition. Then, due to the decreasing property of the exponential function, the depth of the HCBL sizes, in the normal direction $\boldsymbol{e}_1$ of the boundary Γ_m can be estimated by $d_m = \frac{3}{\delta_m}$. In practice, the determination of the length d_m can be performed numerically according to empirical trial and error calculations. It is shown in Appendix B, how the parameters δ_m and the functions $\Psi^m_i(y)$ are found to be solution of the following eigenvalues problem, for both cases considered here. The solutions are computed such that:

- in the truncated sub-domain $\widetilde{G}_m$,

$$\delta^2_m \boldsymbol{k}_{11}\Psi^m_i - \delta_m\left[\left(\frac{\partial \boldsymbol{k}_{11}}{\partial y_1}\right) + \frac{\partial \boldsymbol{k}_{12}}{\partial y_2} + \frac{\partial \boldsymbol{k}_{13}}{\partial y_3}\right]^m_i + div_y\ \boldsymbol{K}\nabla_{\boldsymbol{y}}(\Psi^m_i) - 2\delta_m \begin{bmatrix} k_{11} \\ k_{12} \\ k_{13} \end{bmatrix}^t \boldsymbol{K}\nabla_{\boldsymbol{y}}(\Psi^m_i) = 0 \text{ in } \widetilde{G}_m \tag{21.a}$$

$$\Psi^m_i(y) \quad \text{Periodic in the } \boldsymbol{e}_2, \boldsymbol{e}_3 \quad \text{directions} \tag{21.b}$$

- with the boundary conditions:
  1. Neumann or Fourier conditions, ($m = 2,3$):

$$\boldsymbol{K}(\boldsymbol{y})(\nabla_{\boldsymbol{y}}\boldsymbol{\Psi}^{\boldsymbol{m}}_{\boldsymbol{i}}(\boldsymbol{y})) \cdot \boldsymbol{n} = \boldsymbol{e}exp(-\delta_m y_1)[-\boldsymbol{K}(\boldsymbol{y})(\boldsymbol{e_j} + \nabla_{\boldsymbol{y}}\boldsymbol{\omega_j}(\boldsymbol{y})) + \frac{1}{|Y|}\int_Y \boldsymbol{K}(\boldsymbol{y})(+\nabla_{\boldsymbol{y}}w_j(\boldsymbol{y}))\boldsymbol{d}y] + \begin{bmatrix} \delta_m\Psi^m_i \\ 0 \\ 0 \end{bmatrix} \cdot \boldsymbol{n} \quad \text{on } \Gamma'_m, \tag{21.c}$$

  2. Dirichlet condition ($m = 1$)

$$\Psi^m_i(\boldsymbol{y}) = e^{-\delta_1(L_1 - y_1)}\omega_j(\boldsymbol{y}) \quad \text{on } \Gamma'_1 \tag{21.d}$$

3. Numerical results – discussion

The mathematical homogenization developed above, lead to the determination on one hand of the effective conductivity tensor $\boldsymbol{K}^*$ of the homogenized medium and to boundary layer terms $T^1_{BL}(\boldsymbol{x},\boldsymbol{y})$ which are correcting terms of the first order in the asymptotic expansion of the homogenized solutions, on the other hand.

To illustrate these results, two numerical examples are developed: one is a simple periodic multilayered structure and the other one is a unidirectional composite which involves parallel cylindrical fibers within an insulating polymer matrix. The effective conductivity tensors of the homogenized medium, together with the boundary correcting terms corresponding to the different kinds of boundary conditions are computed. Thus the heterogeneous and the homogenized solutions (temperature and heat flux) are compared. Numerical solutions are computed using the Finite Element Software Comsol Multiphysics®. Moreover, the homogenization process allows to reduce significantly the node number and the degree of freedom (dof) number, required for meshing the spatial domain of the heterogeneous medium, without loss of accuracy. They are compared at the end of the Section 3.

3.1. Periodic multilayered structure

Due to the symmetry of the structure and the assumption of periodic conditions on four faces of the parallelepiped as discussed in Section 2, the numerical study can be reduced (Fig. 4a and b) without loss of generality, on a rectangular spatial 2-D domain. The conductivity tensor $\boldsymbol{K}(\boldsymbol{y})$ on the cell domain is denoted

$$\boldsymbol{K}(\boldsymbol{y}) = \begin{bmatrix} \boldsymbol{k}_{11} & 0 \\ 0 & \boldsymbol{k}_{22} \end{bmatrix}, \text{ with } \boldsymbol{k}_{ii}(\boldsymbol{y}) = \begin{bmatrix} \boldsymbol{k_m}, & \text{if } \boldsymbol{y}\epsilon(\textit{layer } 1) \\ \boldsymbol{k_f}, & \text{if } \boldsymbol{y}\epsilon(\textit{layer2}) \end{bmatrix} \quad i = 1,2$$

3.1.1. The homogenized heat conductivity tensor

To compute the terms of the homogenized heat conductivity tensor $\boldsymbol{K}^*$ (see Section 2.2), the functions w_i, $i = 1,2$, are first determined on the cell domain $\boldsymbol{Y}$, with the data given in Table 1. The multilayered stack is characterized by the thickness $l/2$ of each layer, and the thermal contrast $\kappa = k_f/k_m$, the ratio of the heat conductivity of the conductive layer over the insulating one. An analytical resolution shows that the functions w_i, $i = 1,2$, are independent of the y_1 variable:

$$\boldsymbol{w}(\boldsymbol{y}) = \begin{cases} w_1(\boldsymbol{y}) = 0 \\ w_2(\boldsymbol{y}) = \left[\int_0^l \frac{d\xi}{k_{22}(\xi)}\right]^{-1} \int_0^{y_2} \frac{d\xi}{k_{22}(\xi)} - y_2 \end{cases}$$

Then the components of the homogenized conductivity tensor are computed according to Eq. (6). The numerical values which quantify the non isotropic property of the homogenized medium, are found to be:

$$\boldsymbol{K}^* = \begin{bmatrix} k^*_{11} & k^*_{21} \\ k^*_{12} & k^*_{22} \end{bmatrix} = \begin{bmatrix} 2.6 & 0 \\ 0 & 0.38 \end{bmatrix} \quad (\mathrm{W.m^{-1}.K^{-1}}) :$$

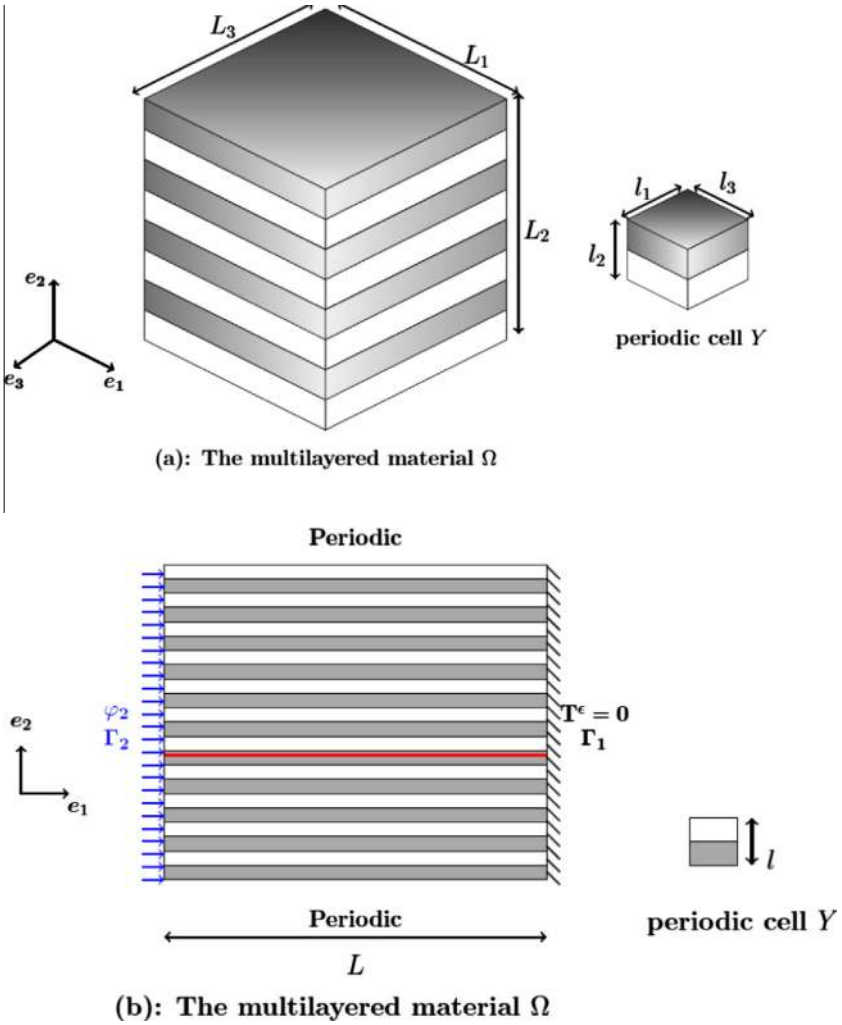

Fig. 4. The multilayered medium and its periodic cell – (a) 3-D domain; (b) 2-D domain – Insulting layer (grey), conductive layer (blank).

Table 1
Thermal and geometrical data for the multilayered structure.

Layer	Property	Value
Layer 1	k_m (W · m^{-1} · K^{-1})	0.2
Layer 2	k_f (W · m^{-1} · K^{-1})	5
	L (mm)	10
Geometry	l (mm)	1
	ϵ	0.1

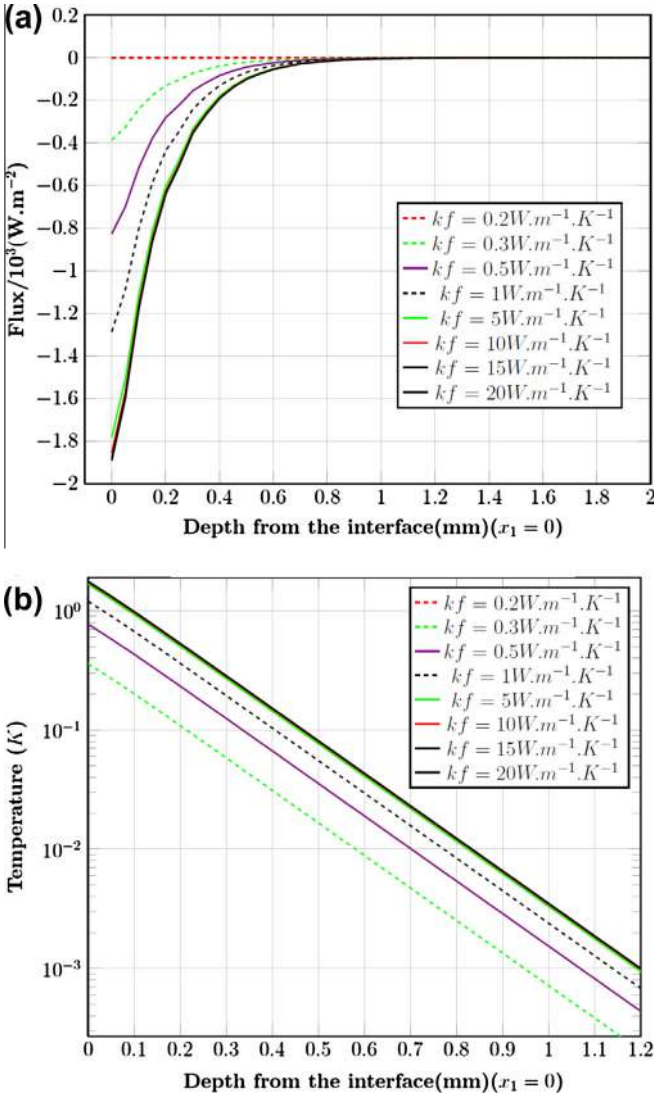

Fig. 5. Influence of the thermal contrast k_f/ k_m on the correcting terms $T_{BL}{}^{1,2}$ and ϕ^0_{BL}, computed on the sub-domain $\widetilde{G}_2$, truncated at $d_2 = 2$ mm; (a): Heat flux ϕ^0_{BL}; (b): Temperature $T_{BL}{}^{1,2}$ (in the insulating layer, i.e. along the red line drawn on Fig. 4b).

It can be noted that, in this simple multilayered case, these values can be easily found by using standard heat conduction rules: $k^*_{11} = \frac{k_m + k_f}{2}$, $\frac{1}{k^*_{22}} = \frac{1}{2}\left(\frac{1}{k_m} + \frac{1}{k_f}\right)$.

3.1.2. Correcting term and Boundary layer associated to a Dirichlet boundary condition

To compute the boundary layer term $T_{\mathrm{BL}}{}^{1,1}(\boldsymbol{x},\boldsymbol{y})$, in the vicinity of the boundary Γ_1, associated to the Dirichlet condition, the method developed in Section 2.3.2 is performed numerically. The functions $\chi^1_i(\boldsymbol{y})$, $i = 1, 2$, solutions of the elementary problems, set on

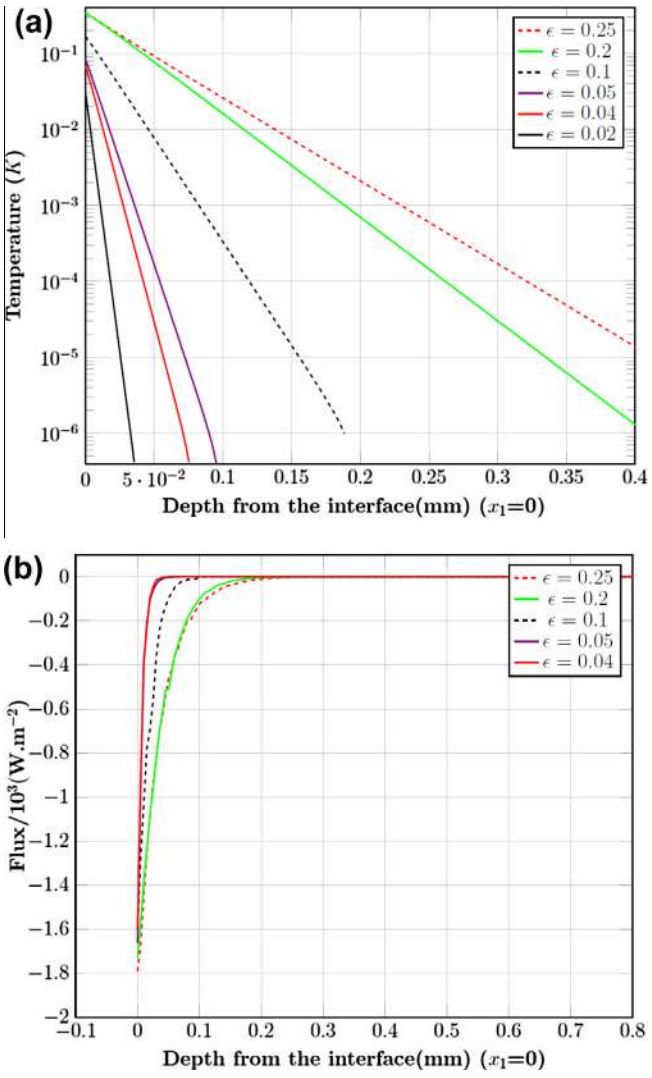

Fig. 6. Influence of the scale ratio ε on the correcting terms $T_{BL}{}^{1,2}$ and ϕ^0_{BL}.e1, versus x_1, computed on the sub-domain $\widetilde{G}_2$, truncated at $d_2 = 0.8$ mm/ (a): temperature $T_{BL}{}^{1,2}$/ (b): Heat flux density $\phi^0_{BL} \cdot e_1$ (in the insulating layer, i.e. along the red line drawn on Fig. 4b). (For interpretation of the references to color in this figure legend, the reader is referred to the web version of this article.)

the truncated sub-domain $\widetilde{G}_1 =]L - d_1, L] \times]0, l] \times]0, l]$, are first computed with $d_1 = 2$ mm from Γ'_1. The function $\chi^1_1(\boldsymbol{y})$ is equal to zero. Because of the periodic boundary conditions taken in the e_2 direction, the component of the thermal gradient $\frac{\partial T^0}{\partial x_2}$ is also equal to zero, then the correcting term $T^{1,1}_{BL}$ in this example is the sum of two terms which are equal to zero, everywhere in $\widetilde{G}_1$. Consequently, the correcting term $\boldsymbol{\phi}^{0,m}_{BL}$ is also null:

$$\phi^{0,m}_{BL}(\boldsymbol{x},\boldsymbol{y}) = K(y)(\nabla_{\boldsymbol{y}}\boldsymbol{\chi}^m(y)).\nabla_x \boldsymbol{T}^0(\boldsymbol{x}) = 0$$

This example illustrates a particular case, where edge effects are null; the first order approximation $T^0(\boldsymbol{x}) + T^1(\boldsymbol{x},\boldsymbol{y})\,\epsilon$ of the heterogeneous solution does not require any edge correction, and gives accurate results even close to this boundary.

3.1.3. Correcting term and Boundary layer associated to a Neumann boundary condition

To compute the boundary layer term $T^{1,2}_{BL}(\boldsymbol{x},\boldsymbol{y})$, in the vicinity of the boundary Γ_2, associated to a Neumann condition, the method developed in Section 2.3.1 is performed numerically. The functions $\chi^2_i(\boldsymbol{y})$, $i = 1, 2$, are firstly computed by solving the following elementary problems, set on the sub-domain $\widetilde{G}_2$, Eqs. (10.a)–(10.b),

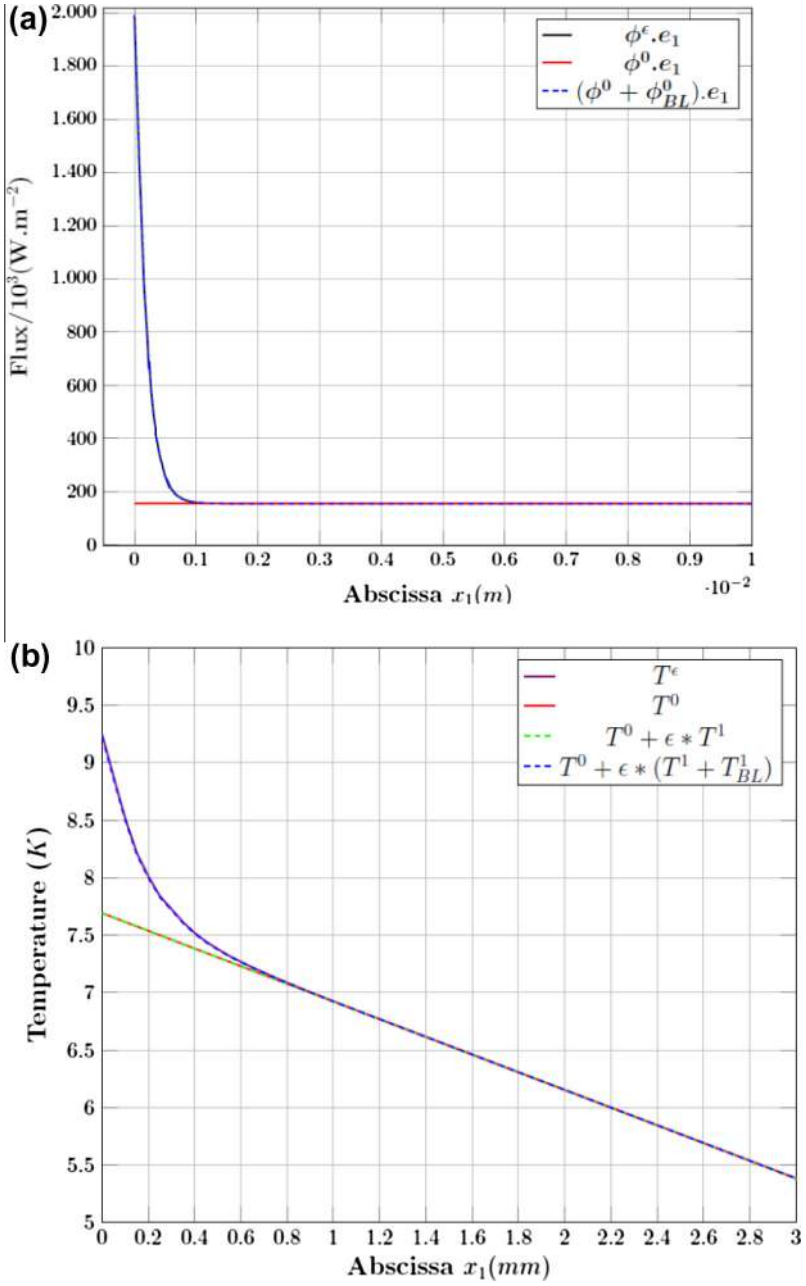

Fig. 7. Comparison of homogenized and heterogeneous fields in the insulating layer (along the red line, Fig. 4b), computed on the sub-domain $\widetilde{G}_2$, truncated at $d_2 = 3$ mm/ (a): Heat flux density/ (b): Temperature fields. (For interpretation of the references to color in this figure legend, the reader is referred to the web version of this article.)

on the sub-domain $\widetilde{G}_2 =]0, d_2[\times]0, l[\times]0, l[$, truncated at the distance $d_2 = 2$ mm from Γ'_2, in the normal direction $\boldsymbol{e}_1$.In this example, the function $\chi^2_2(\boldsymbol{y}) \equiv \boldsymbol{0}$, is equal to zero, then the boundary layer term $T^{1,2}_{BL}(\boldsymbol{x},\boldsymbol{y})$ reduces to

$$T^{1,2}_{BL}(\boldsymbol{x},\boldsymbol{y}) = \frac{\partial T^0}{\partial x_1}(\boldsymbol{x})\chi^2_1(\boldsymbol{y})$$

From the numerical solution of the eigenvalues problem (see Section 2.4.1), the lowest solution is found to be $\delta_2 = 6277$ m^{-1} and the estimation of the boundary layer depth is $d_2 \approx \frac{3}{\delta_2} = 0.5$ mm. Then the influence of the thermal contrast on the depth of the boundary layer d_2 can be easily studied by solving numerically the eigenvalues problem for several values of the thermal contrast k_f/k_m. It is found that the value of d_2 is independent from this parameter. Fig. 5a and b show the boundary layer terms $T^{1,2}_{BL}$ and $\boldsymbol{\phi}^0_{\boldsymbol{BL}}$ computed for several values of k_f, while the value $k_m = 0.2$ - $\mathrm{W \cdot m^{-1} \cdot K^{-1}}$is kept constant. Two results are highlighted from these plots: (i) the variation of the thermal contrast has no influence on the boundary layer size; (ii) only the magnitude of $T^{1,2}_{BL}$ and $\boldsymbol{\phi}^0_{\boldsymbol{BL}}$ increases with the thermal contrast up to a limit $k_f/k_m = 25$, and no influence is observed over this limit.

In the same way, the influence of the scale ratio ε on the depth of the boundary layer can be easily studied. Fig. 6a and b depict the evolution of $T^{1,2}_{BL}$ and $\boldsymbol{\phi}^0_{\boldsymbol{BL}}$ along x1 for different values of ε. We first observe that the boundary layer term $T^{1,2}_{BL}$ tend to become negligible when ε decreases, contrary to the heat flux $\boldsymbol{\phi}^0_{\boldsymbol{BL}}$. These results confirm that the edge effect correction is not necessary for the

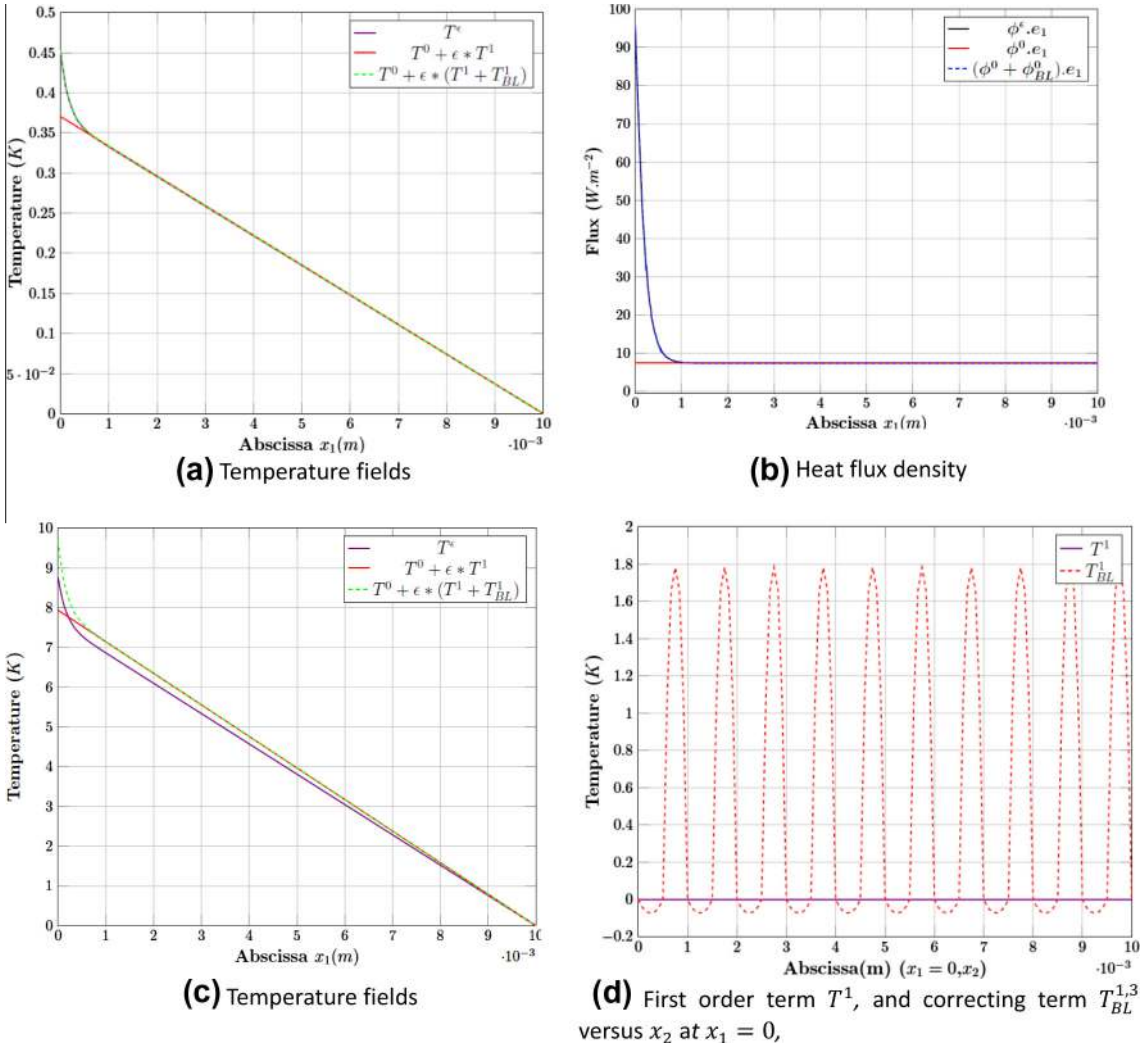

Fig. 8. Comparison of homogenized and heterogeneous fields (8(a)–(c)) in the insulating layer (along the red line, Fig. 4b). Influence of the heat transfer coefficient, 8(a) and (b): h = 10 W/m^2 K, and 8(c) and (d): h = 1000 W/m^2 K. (For interpretation of the references to color in this figure legend, the reader is referred to the web version of this article.)

temperature field when ε is small enough (T^0 is thus a good approximation of T^ϵ). However, this correction has to be applied from the order 0 of ε to the heat flux, since heat flux density is sensitive to edge effect even for small values of the scale ratio.

Finally to underline the importance of the correcting terms close to the boundary, it is interesting to compare the computed solutions of the heterogeneous and homogenized fields of temperature and heat flux density. The following heat flux is thus applied on Γ_2: $\boldsymbol{\varphi}^\epsilon(s) \cdot \boldsymbol{n} = \varphi_2 = 2.10^3$ Wm^{-2}. The comparison is done along a 1D cut (see red line in Fig. 4c) in a insulating layer, on Fig. 7. Let us recall that the exact temperature $T(x)$ in a homogeneous 1-D wall (without edge effect), computed with a Dirichlet condition $T = 0$ at $x_1 = L_1$, and a Neumann condition at $x_1 = 0$ and the heat conductivity coefficient k^*_{11} is

$$T(x_1) = -\frac{\varphi_2}{\frac{k^*_{11}}{L_1}}\left(\frac{x_1}{L_1} - 1\right).$$

In this example, the temperature predicted by the approximation $T^0(0,x_2) + T^1(0,x_2)\varepsilon$ at ($x_1 = 0$), without correcting term, is independent of the x_2 variable and is identical to the exact homogeneous medium solution, the computed value is $T(0) = 7.69$ K, as shown on Fig. 11b. Moreover, $\frac{dT^\epsilon}{dx_1}$ the slope of the heterogeneous field within the wall, far enough from the boundary (see Fig. 11b), is constant and identical to that of the homogeneous one $\frac{dT}{dx_1} = -\frac{\varphi_2}{k^*_{11}}$ computed with the effective heat conductivity k^*_{11} in the direction $\boldsymbol{e}_1$.

These curves illustrate how the approximation at the first order of the temperature $T^0(\boldsymbol{x}) + T^1(\boldsymbol{x},\boldsymbol{y})\cdot\epsilon$ and heat flux density $\boldsymbol{\phi}^0(\boldsymbol{x},\boldsymbol{y})\cdot\boldsymbol{e}_1$ computed for the homogenized medium are good approximations respectively of the temperature $T^\epsilon(x)$ and heat flux $\boldsymbol{\phi}^\epsilon(\boldsymbol{x})\cdot\boldsymbol{e}_1$ of the heterogeneous medium, provided that $\boldsymbol{x} \in \Omega$ is far enough from the boundary Γ_2 (in the normal direction to this boundary). In the vicinity of the boundary Γ_2, additional terms are needed to correct the edge effects, thus the approximations $T^0(\boldsymbol{x}) + (T^1(\boldsymbol{x},\boldsymbol{y}) + T^1_{BL}(\boldsymbol{x},\boldsymbol{y}))\varepsilon$ and $\boldsymbol{\phi}^0(\boldsymbol{x},\boldsymbol{y}) + \boldsymbol{\phi}^0_{\boldsymbol{BL}}(\boldsymbol{x},\boldsymbol{y})$ have to be considered and give accurate results.

3.1.4. Correcting term and boundary layer associated to a Fourier condition

It was shown in Section 2.3.2 and Appendix A, how the same approach can be used to compute the boundary layer term $T^{1,3}_{BL}(x,y)$, in the vicinity of the boundary Γ_3, associated to a Fourier condition $\boldsymbol{\varphi}^\epsilon(s)\cdot\boldsymbol{n} = h(T^\epsilon - T_{ext})$ on Γ_3. The numerical method is thus applied. The functions $\chi^3_i(\boldsymbol{y})$, $i = 1, 2$, being identical (in this example) to those computed for the Neumann condition $\chi^2_i(\boldsymbol{y}), i = 1, 2$, see the Fig. 8.a, hence the influence of the thermal contrast, or the scale ra-

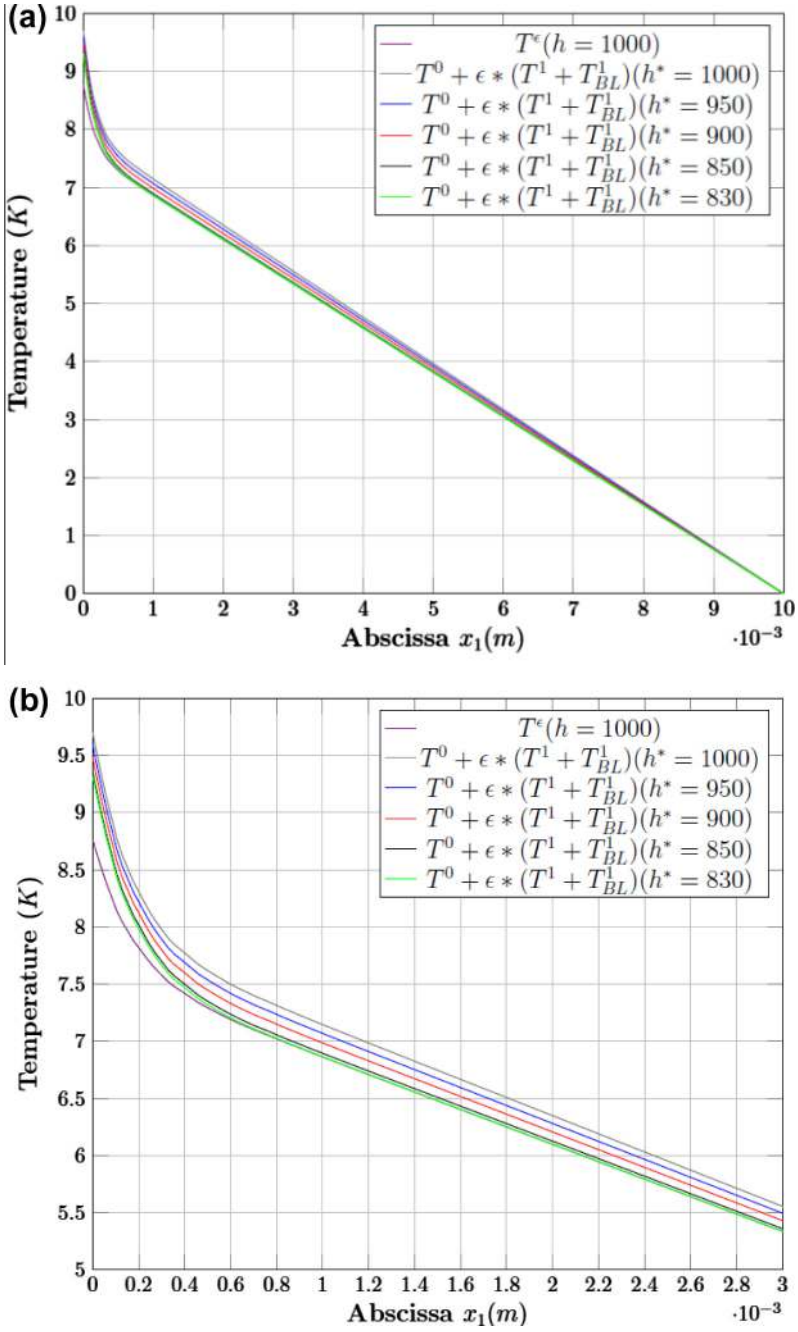

Fig. 9. Comparison of homogenized and heterogeneous temperature fields in the insulating layer (along the red line, Fig. 4b). Influence of the modified heat transfer coefficient. (For interpretation of the references to color in this figure legend, the reader is referred to the web version of this article.)

tio on the correcting term $T^{1,3}_{BL}(\boldsymbol{x},\boldsymbol{y})$, in the vicinity of the boundary Γ_3, are similar.

However, the main difference with the Neumann condition comes from the introduction of the heat transfer coefficient h and the external temperature T_{ext}. For numerical application, it is taken here to the value $T_{ext} = 10K$. Then it is interesting to illustrate the influence of the coefficient h on the homogenized solution with or without the correcting term $T^{1,3}_{BL}$. Homogenized and heterogeneous fields, computed along the 1-D cut red line shown on Fig. 4c, (insulating layer) are compared on Fig. 12, for the values $h = 10\ \mathrm{W/m^2\ K}$ and $h = 1000\ \mathrm{W/m^2\ K}$. The exact temperature $T(x)$ in a homogeneous 1-D wall (without edge effect), computed with a Dirichlet condition $T = 0$ at $(x_1 = L_1)$, a Fourier condition at $(x_1 = 0)$ and the heat conductivity coefficient k^*_{11}, is now $T(x) = -\frac{T_{ext}}{1+\frac{k^*_{11}}{hL_1}}\left(\frac{x_1}{L_1}-1\right)$, thus the temperature at $(x_1 = 0)$ satisfies:

$$T(0) = \frac{T_{ext}}{1+\frac{k^*_{11}}{hL_1}} < T_{ext}$$

- *For* $h = 10\ \mathrm{W/m^2\ K}$, Fig. 8a and b, the values taken by the approximated solution without correcting term, $T^0(0,x_2) + T^1\ (0,x_2)\varepsilon$, are independent of the variable x_2. As shown on Fig. 8a, they are identical to the predicted value $T(0) = 0.37$ K, Moreover, the slope of the heterogeneous field inside the wall, on the Fig. 8a, is almost identical to that of the analytical one: $\frac{dT^{\varepsilon}}{dx_1} \approx \frac{dT}{dx_1} = -\frac{\varphi_2}{k^*_{11}}$

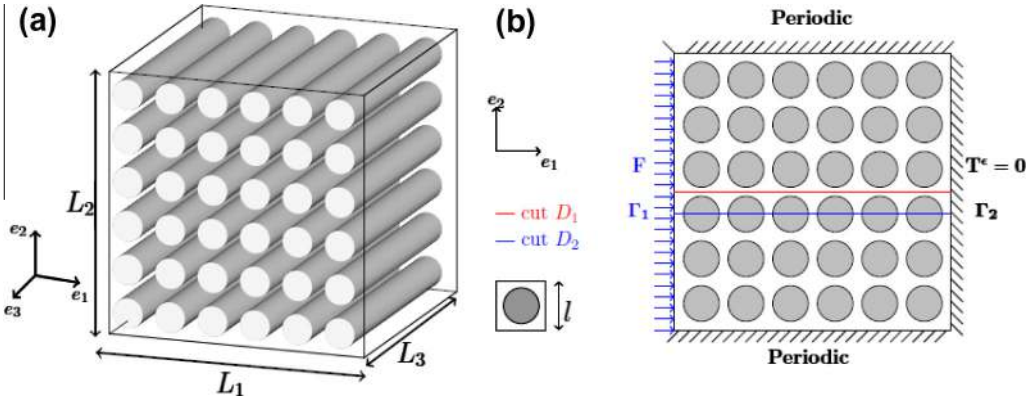

Fig. 10. The matrix/fiber composite medium and its periodic cell – (a) 3-D domain; (b) 2-D domain.

Table 2
Thermal and geometrical data for the matrix/fiber composite structure.

Components	Property	Value
Matrix	k_m ($W \cdot m^{-1} \cdot K^{-1}$)	0.2
Fiber	k_f ($W \cdot m^{-1} \cdot K^{-1}$)	5
	L (mm)	10
Geometry	l (mm)	1
	The fiber ratio (τ_f)	0.64
	ϵ	0.1

Table 3
Influence of the thermal contrast and the fiber ratio on the effective heat conductivity.

The thermal contrast	The fiber ratio	Asymptotic expansion method k_{11}^*
10	0.20	1.391
	0.55	2.695
50	0.20	1.476
	0.55	3.373
100	0.20	1.488
	0.55	3.487

- For $h = 1000\ W/m^2\ K$, Fig. 8c and d, we get $T(0) = 7.93$ K, it is also the value obtained from the approximated solution without correcting term $T^0(0,x_2) + T^1(0,x_2)\varepsilon$, shown on Fig. 8c, and the slope of the approximated field remains close to the exact value $\frac{d(T^0(x)+T^1(x)\varepsilon)}{dx_1} \approx \frac{dT}{dx_1}$. However, in that case, the temperature slopes of the heterogeneous and homogeneous wall inside the wall (Fig. 8c) are clearly different:

$$\frac{\partial T^\varepsilon}{\partial x_1} \neq \frac{dT}{dx_1} = -\frac{T_{ext}}{1+\frac{k_{11}^*}{hL_1}}\frac{1}{L_1}$$

This deviation can be explained by the fact that the approximation T^0 is computed without taking into account the edge effect (see Section 2.2). Consequently the average heat flux which enters the wall through Γ_3', is only an approximation of the true value and it is over-predicted:

$$\frac{h}{l}\int_0^l \Big(T_{ext} - T^0(0,x_2)\Big)dx_2 > \frac{h}{l}\int_0^l (T_{ext} - T^\varepsilon(0,x_2))dx_2$$

This heat flux bias inside the wall, between $k_{11}^*\frac{dT^\varepsilon}{dx_1}$ and $k_{11}^*\frac{d(T^0(x)+T^1(x)\varepsilon)}{dx_1}$ is well illustrated by the slope difference, on Fig. 8.c. The heat flux entering the wall in a homogeneous medium, without edge effect, would be:

$$-k_{11}^*\frac{dT}{dx_1} = \frac{T_{ext}}{1+\frac{k_{11}^*}{hL_1}}\frac{k_{11}^*}{L_1} = \frac{T_{ext}}{\frac{L_1}{k_{11}^*}+\frac{1}{h}}$$

And we note that $R_{hom} = \frac{L_1}{k_{11}^*} + \frac{1}{h}$ defines the thermal resistance of the homogeneous wall.

To correct the heat flux bias in this example, we suggest to change the thermal resistance for computing $T^0(\boldsymbol{x})$. This can be done by changing the heat transfer coefficient h by a modified value h^* in the boundary condition on Γ_3. Eq. (3.d) becomes:

$$\langle \boldsymbol{\varphi}^0 \rangle \cdot \boldsymbol{n} = h^*(T^0 - T_{ext}) \quad \text{on } \Gamma_3,$$

And the modified value h^* is determined in order to have a better heat flux prediction through Γ_3':

$$h^*\int_0^l (T_{ext} - T^0(0,x_2))dx_2 \cong h\int_0^l (T_{ext} - T^\varepsilon(0,x_2))dx_2$$

Then the modified thermal resistance of the heterogeneous 1-D wall becomes:

$$R_{het} = \frac{L_1}{k_{11}^*} + \frac{1}{h^*}$$

The thermal resistance difference between the heterogeneous and the homogeneous media, due to the thermal constriction phenomenon generated at the boundary Γ_3 by the multilayered periodic structure. named R_{const}, is then

$$R_{const} = R_{het} - R_{hom} = \frac{1}{h^*} - \frac{1}{h}$$

A numerical value of the modified heat transfer coefficient h^* can be computed as follows:

- an initial guess is taken: $h^* = h$
- then $T^0, T^1 + T_{BL}^{1,3}$, are computed to get an approximated solution of T^ε:

$$T^\varepsilon \approx T^0 + \varepsilon\Big(T^1 + T_{BL}^{1,3}\Big)$$

The modified value h^* is then chosen in order to have:

$$h^*\int_0^l \Big(T_{ext} - T^0(0,x_2)\Big)dx_2 = h\int_0^l (T_{ext} - T^0(0,x_2) - T^\varepsilon(0,x_2) + T^0(0,x_2))dx_2$$

which implies:

$$h^*\int_0^l (T_{ext} - T^0(0,x_2))dx_2 \approx h\int_0^l \Big(T_{ext} - T^0(0,x_2) - \varepsilon(T^1 + T_{BL}^{1,3})\Big)dx_2$$

$$h^* \approx h\left[1 - \varepsilon\frac{\int_0^l \Big(T^1(0,x_2) + T_{BL}^{1,3}(0,x_2)\Big)dx_2}{\int_0^l (T_{ext} - T^0(0,x_2))dx_2}\right]$$

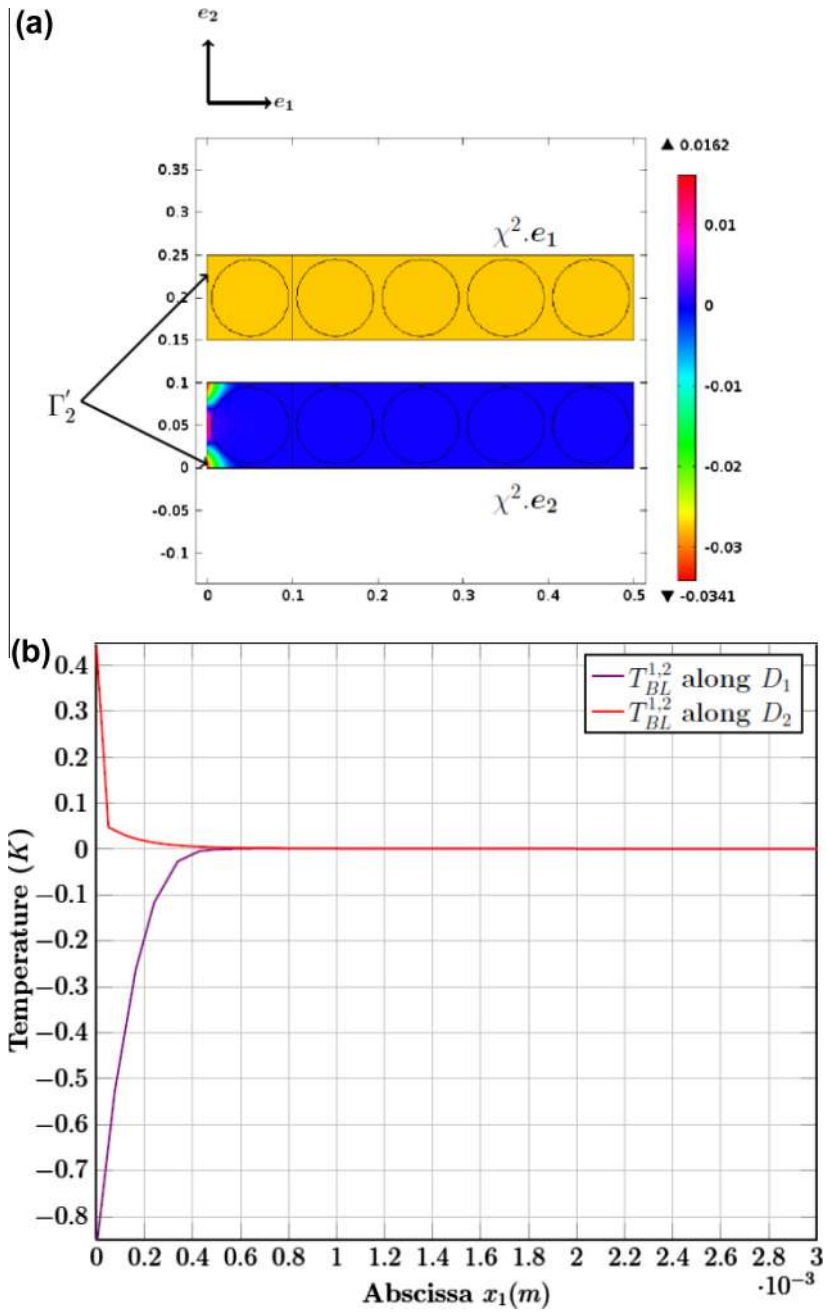

Fig. 11. Numerical solutions/ (a): $\chi_i^2(y),\ i = 1,2$ computed on $\widetilde{G}_2$, truncated at $d_2 = 0.5$ mm and/ (b): ${T_{BL}}^{1,2}$ along two lines cut (see Fig. 10) on $\widetilde{G}_2$, truncated at $d_2 = 3$ mm.

For example with $h = 1000$ W/m^2 K, the ratio of integrals is positive, then it comes $h^* < h$. The comparison between the heterogeneous solution with the homogenized solutions computed for $h^* < h$, is shown on the Fig. 9: the heat flux bias can be decreased inside the wall with the modified value $h^* = 830$ W/m^2 K.

Finally, this example illustrates the interest in the determination of the correcting term $T_{BL}^{1,3}$ associated to a Fourier condition on the boundary Γ_3. It gives a straightforward way to estimate numerically the thermal constriction resistance $R_{const} = R_{het} - R_{hom}$ generated at the boundary of the heterogeneous medium, without computing the heterogeneous field T^ε. In this example, the value is evaluated to:

$$R_{const} = \frac{1}{h^*} - \frac{1}{h} \approx 2.10^{-4} m^2 K/W.$$

It must be noted that the influence of the thermal constriction phenomenon in the studied case, was not discussed above with the Neumann condition. In fact, the constriction effect exists, and the slopes temperature for the homogeneous and the heterogeneous wall with thermal constriction (edge effect) are respectively:

$$\frac{dT}{dx_1} = -\frac{\varphi_2}{k_{11}^*} = -\frac{\varphi_2}{L_1}\left[\frac{L_1}{k_{11}^*}\right] \quad \text{and} \quad \frac{d\overline{T}^\varepsilon}{dx_1} = -\frac{\varphi_2}{L_1}\left[\frac{L_1}{k_{11}^*} + R_{const}\right]$$

so the difference is $\frac{d(\overline{T}^\varepsilon - T)}{dx_1} = -\frac{\varphi_2}{L_1} R_{const}$, which gives $\frac{\overline{T}^\varepsilon(0) - T(0)}{L_1} \approx \frac{0.4K}{L_1}$. It means that the difference between the average value of the heterogeneous temperature $\overline{T}^\varepsilon(0)$ at the boundary, computed on Γ'_2, and the homogeneous value $T(0)$, should be close to 0.4 K. From the first order approximation of the homogenized solution, this difference is

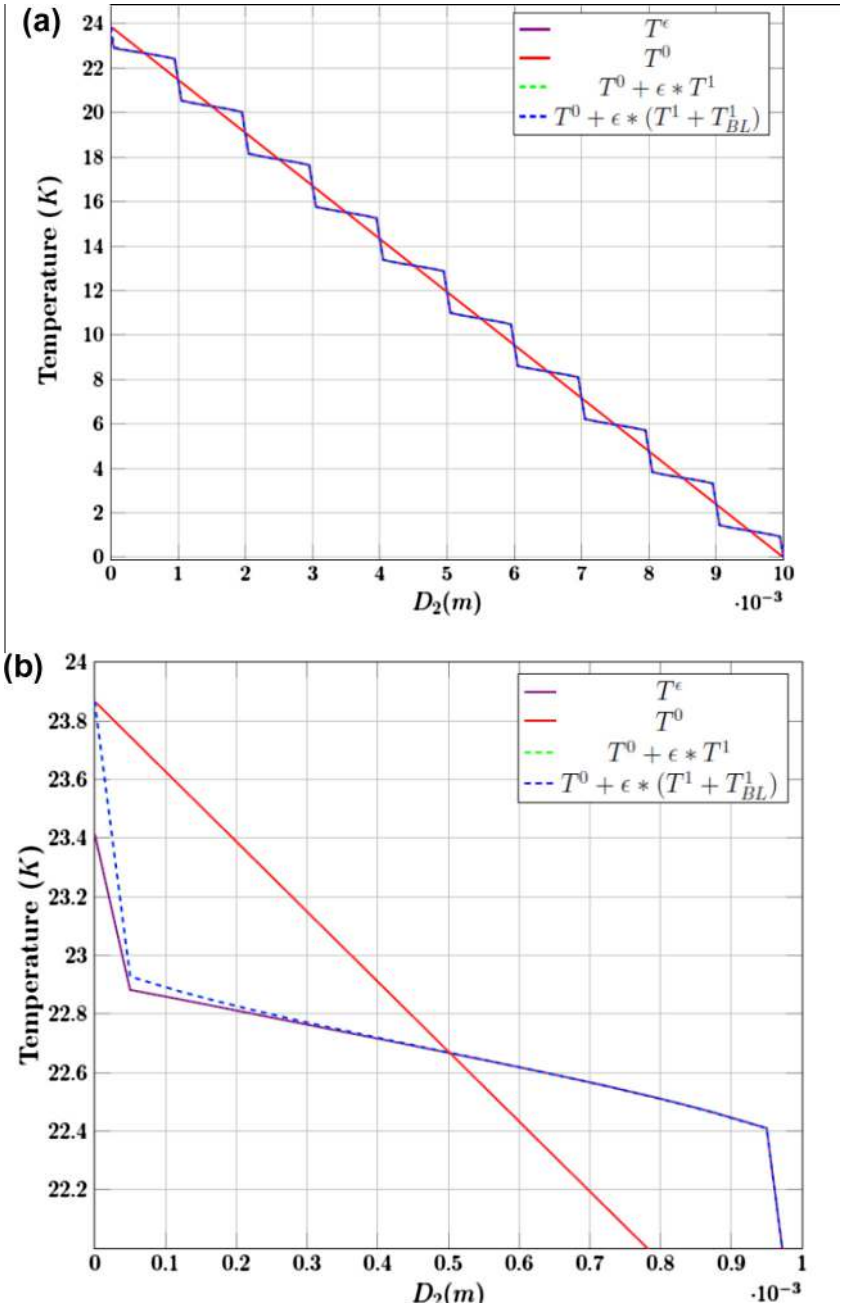

Fig. 12. Comparison of homogenized and heterogeneous temperature fields along the line cut D_2, (see Fig. 10).

given by $\varepsilon(T^1(0,x_2) + T^{1,2}_{BL}(0,x_2))$, and the numerical computation of the term $\frac{\varepsilon}{l}\int_0^l (T^1(0,x_2) + T^{1,2}_{BL}(0,x_2))dx_2 \approx 0.4$ K confirms this value.

In summary, the approach presented in the paper with the boundary layer terms provides satisfying results for Dirichlet or Neumann boundary conditions. This may be not the case for the Fourier boundary condition, depending on the value of the exchange coefficient. On way to overcome this problem is to propose to use a corrected value of exchange coefficient (h^*) to obtain a good approximation of the heterogeneous solution.

3.2. Application to a unidirectional matrix/fiber composite

Following the same approach than in the previous section, numerical computations are performed to illustrate the homogenization method in the case of a composite medium with 3-D periodic structure, as shown of the Fig. 10a. As in the previous example, the numerical study is reduced on a rectangular spatial 2-D domain, Fig. 10b. For simplicity, the property of the medium in the $\boldsymbol{e}_1$ direction, parallel to the fibers will be ignored.

The computed solutions will be plotted along two lines cut in the $\boldsymbol{e}_1$ direction: the red line (D_1) which is entirely in the matrix, and the blue line (D_2) which cuts the fibers. The periodic cell is defined by a circle (radius r_f) within a square *lxl*. The ratio $\tau_f = \frac{\pi r_f^2}{l^2}$ is called the "volume fiber ratio", and $\kappa = \frac{k_f}{k_m}$ the thermal contrast.

3.2.1. The homogenized conductivity tensor-

To compute the terms of the homogenized heat conductivity tensor $\boldsymbol{K}^*$, the functions $\boldsymbol{w}_i$, $i = 1,2$, are first determined on the cell domain Y, with the data given in Table 2. Due to the symmetry of

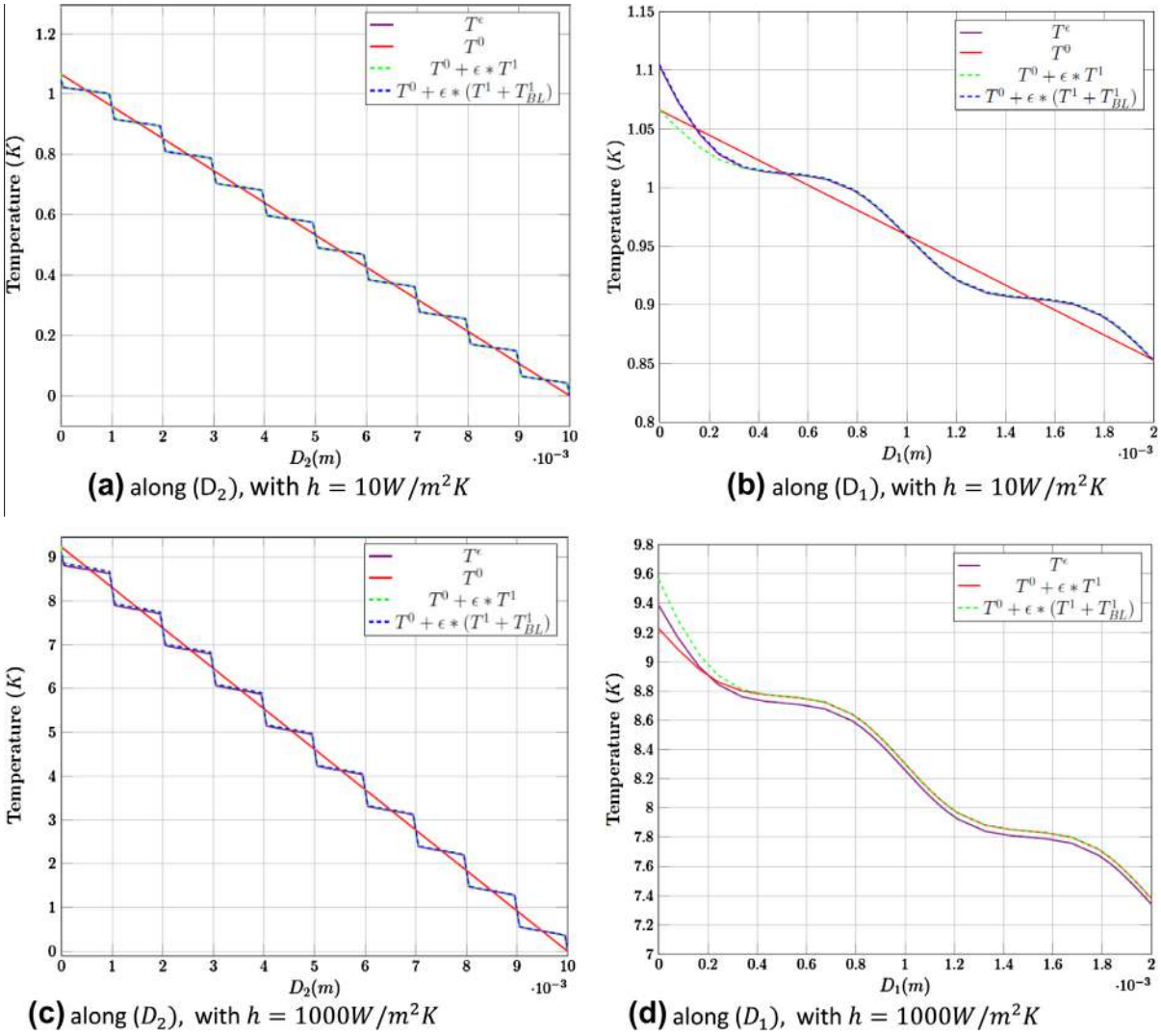

Fig. 13. Comparison of the homogenized and heterogeneous temperature fields: (13(a) and (c)) along (D_2) and (13(b) and (d)) along (D_1) close to the boundary $x_1 = 0$; (13(a) and (b)) with $h = 10$ W/m^2 K and (13(c) and (d)) with $h = 1000$ W/m^2 K.

the cell, the functions $w_1(y) \equiv w_2(y)$ are identical. The homogenized medium is isotropic in the plane $(0, e_1, e_2)$. The components of the homogenized conductivity tensor are identical, they are:

$$k^*_{11} = k^*_{22} = 0.835 \text{ W/mK}.$$

Table 3 shows the influence of the parameters τ_f and κ, on the computed effective heat conductivity. The influences of the thermal contrast and volume fiber ratio, the heat conductivity of the isotropic homogenized medium can be thus easily computed. More general results have been performed by Matine [31] to take into account non perfect thermal contact between the matrix and the fibers. They include the influence of the thermal resistance between the matrix and the fiber, in the computation of the heat conductivity of the homogenized medium.

3.2.2. Correcting term associated to a Neumann boundary condition

The correcting term $T^{1,2}_{BL}(\boldsymbol{x}, \boldsymbol{y})$, Fig. 11b, in the vicinity of the boundary Γ_2, associated to the Neumann condition, is given by the functions $\chi^2_i(y), i = 1, 2$, which are first computed on the sub-domain $\overline{G_2} =]0,\ d_2[\times]0, l[\times]0, l[$, truncated at the distance $d_2 = 0.5mm$ from Γ'_2, in the normal direction e_1.They are plotted on Fig. 11a. The depth of the boundary layer is observed close to

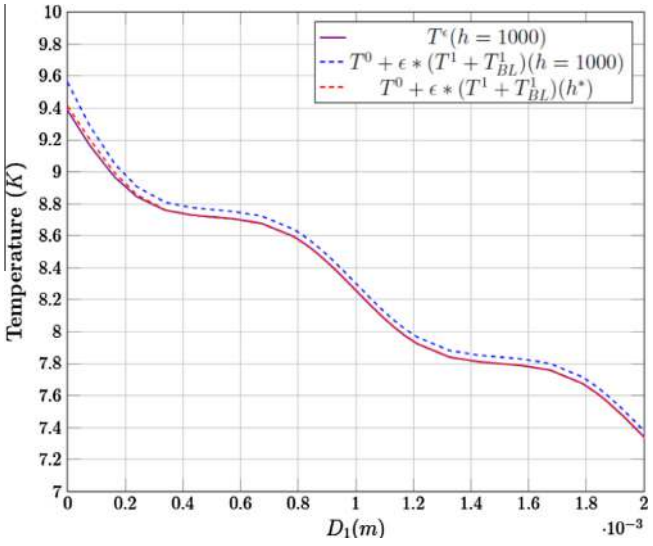

Fig. 14. Heterogeneous Temperature field along the line cut (D_1),computed with $h = 1000$ W/m^2 K, compared to the homogenized approximation, computed with the modified heat transfer coefficient $h^* = 939$ W/m^2 K.

$d_2 = 0.5$ mm. The value is confirmed by the solution of the eigenvalues problem, which gives the lowest computed eigenvalue:

$$\delta_2 = 5688\ \mathrm{m}^{-1} \Rightarrow d_2 \approx \frac{3}{\delta_2} = 0.53\ \mathrm{mm}$$

Numerical solutions are computed with the heat flux fixed on Γ_2 to $\varphi_2 = 2.10^3\ \mathrm{Wm}^{-2}$. The temperature value at $(x_1 = 0)$ predicted by the homogenized solution $T^0(0) + T^1(0.)\varepsilon$ without correcting term, is almost identical to the value computed for the exact homogeneous medium solution, as shown on Fig. 12a:

$$T(0) = \frac{\varphi_2}{\frac{k^*_{11}}{L_1}} = 23.95\ \mathrm{K},$$

As in the previous example, the thermal constriction effect can be evaluated by computing the average temperature deviation $\overline{T}^{\varepsilon}(0) - T(0) \approx 0.209$ K. This numerical value is almost identical to the value predicted by the correcting term: $\frac{\varepsilon}{l}\int_0^l (T^1(0,x_2) + T^{1,2}_{BL}(0,x_2))dx_2$.

3.2.3. Correcting term associated to a Fourier boundary condition

The homogenized and heterogeneous temperatures, along the line cuts (D_1) and (D_2), computed with $h = 10\ \mathrm{W/m^2\,K}$ and $h = 1000\ \mathrm{W/m^2\,K}$, are compared on Fig. 13. Analog observations with the previous case can be done. For high value of the heat transfer coefficient, there is a temperature bias (and a heat flux bias too!) inside the wall, between the heterogeneous and the homogenized fields. This bias is well illustrated along the line cut (D_1) on Fig. 13.d. Like in the previous example, it can be decreased by modifying the heat transfer coefficient according to the numerical procedure described in Section 3.1.4 from the knowledge of the correcting term $T^{1,3}_{BL}$. For this example, as shown of Fig. 14, the "best" value of the modified coefficient is found to be $h^* = 939\ \mathrm{W/m^2\,K}$. The thermal constriction resistance is then estimated for this heterogeneous structure to

$$R_{cons} = \frac{1}{h^*} - \frac{1}{h} \approx 6.10^{-5}\ \mathrm{m^2K/W}$$

3.2.4. Correcting term associated to a Dirichlet boundary condition

The correcting term $T^{1,1}_{BL}(\boldsymbol{x},\boldsymbol{y})$, Fig. 15b, in the vicinity of the boundary Γ_1, associated to the Dirichlet condition $T_1 = 0$, on Γ_1, is computed from the functions $\chi^1_i(\boldsymbol{y})$, $i = 1,2$, Fig. 15a, on the truncated sub-domain $\overline{G}_1 =]L - d_1, L[\times]0, l[\times]0, l[$, with $d_1 = 2$ mm from Γ'_1. Solving the eigenvalues problem for the determination the boundary layer depth, gives analog results with the Neumann condition problem, the value is observed close to 0.5 mm on Fig. 15b. Contrary to the previous example, the correcting term $T^{1,1}_{BL}$ associated to a Dirichlet boundary condition, is not equal to zero, but remains close to zero. The homogenized solutions $T^0(L_1) + T^1(L_1,y_2)\epsilon$ and $T^0(L_1) + (T^1(L_1,y_2) + T^1_{BL}(L_1,y_2))\epsilon$, computed respectively without and with the correcting term are compared on the boundary Γ_1, Fig. 16.

3.3. Computational costs

For both examples discussed above, heterogeneous and homogenized numerical solutions have been computed with a finite element solver which needs to specify the mesh size of the considered spatial domain. It must be underlined that for getting solutions with similar accuracy, the mesh size needed for the heterogeneous structure are quite different than for the homogenized solution. In Table 4, we summarize the number of nodes and degrees of freedom (dof) used to obtain the results presented in Sections 3.2 and 3.3. The computational cost is proportional to the square of the dof. For each example, five kinds of solutions have been com-

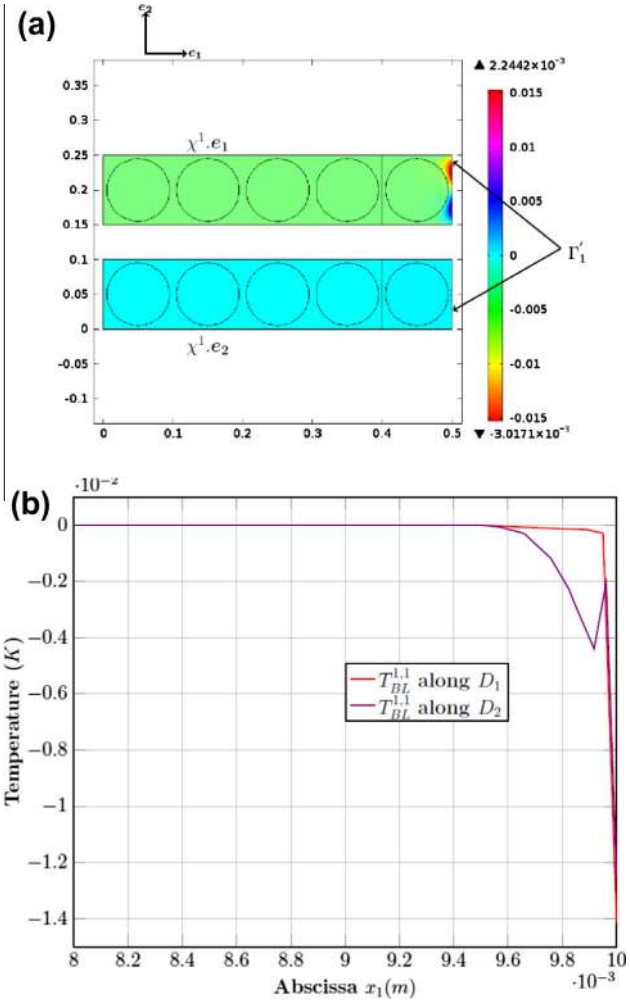

Fig. 15. Numerical solutions/ 15a: $\chi^1_i(y)$, $i = 1,2$ computed on $\widetilde{G}_1$, truncated at $d_1 = 0.5$ mm and/15b: $T_{BL}{}^{1,1}$ along two lines cut (see Fig. 10) on $\widetilde{G}_1$, truncated at $d_1 = 2$ mm.

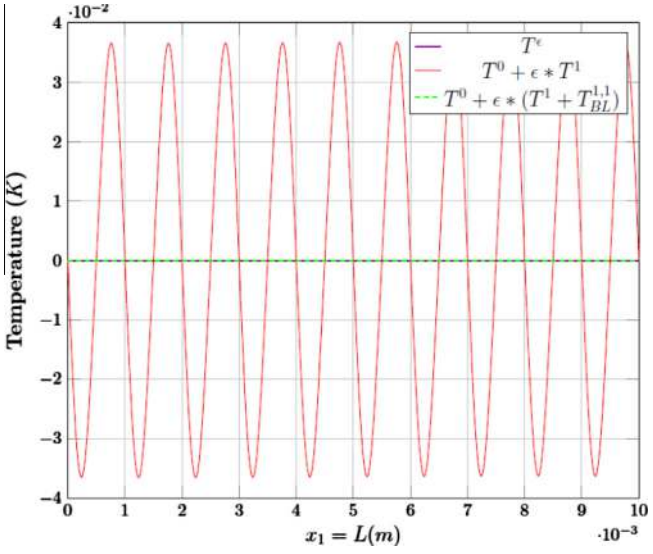

Fig. 16. Comparison of the homogenized temperatures, computed without and with the correcting term $T^{1,1}_{BL}$. The heterogeneous temperature is fixed to $T_1 = 0$, on Γ_1.

Table 4
Mesh data used for computing the numerical solutions with the finite element solver.

Computed solutions	Spatial domain	Example 1 (Section 3.1)		Example 2 (Section 3.2)	
		Node numbers	(dof)	Node numbers	(dof)
$T^{\epsilon}(x)$	Piece Ω	7716	30,551	13,054	51,673
$T^{0}(x)$	Piece Ω	315	1189	336	1281
$w(y)$	Cell Y	S3	454	192	723
$\chi^{m}(y)$	$\widetilde{G}_m$	117	858	401	3809
$\psi_i^{m}(y)$	$\widetilde{G}_m$	117	858	401	3809

puted, and for each of one, we precise the associated mesh and (dof) used.

4. Conclusion

An homogenization approach based on asymptotic expansions, accounting for edge effects has been developed. This method relies on the solutions of three microscopic scale problems and a macroscopic one. The microscopic scale problems provide effective thermal properties, the depth of edge effects and the boundary layer corrections, depending on the kind of boundary conditions considered. These latter can then improve the solution of the homogenized fields at the macroscopic scale. It leads to a good approximation of the solution, even in the vicinity of the boundaries. The accuracy of this approach has been shown through numerical results obtained for two examples: a multilayered material and a composite structure.

For Dirichlet or Neumann boundary conditions, the approach presented in the paper with the boundary layer terms provides satisfying results. The numerical study of the correcting term associated to a Fourier boundary condition, has highlighted the influence of the heat transfer coefficient on the accuracy of the homogenized solutions. The thermal analysis leads to introduce a modified heat transfer coefficient in order to improve the modeling of the homogenized heat flux entering the medium through this boundary. This result can be interpreted by the thermal constriction phenomenon generated on the boundary. It was shown how a thermal constriction resistance can be evaluated directly from the computation of the correcting term.

From the computation point of view, the examples also illustrate how the homogenized approach allows to strongly reducing the number of degrees of freedom in performing the finite element method, comparatively to the resolution over the original heterogeneous medium.

The method presented here is quite general for stationary heat conduction analysis within periodic structures. Moreover, it has already been extended to non periodic heterogeneous medium, such as random one. In such case, the question of the determination of the Representative Elementary Volume (REV) becomes crucial, and can be analyzed with statistical tools. Other extensions of the method are concerned with non stationary heat conduction.

Appendix A. Problem Statement for the determination of correcting terms $T_{BL}^{1,m}(\boldsymbol{x},\boldsymbol{y})$ and $\phi_{BL}^{0}(\boldsymbol{x},\boldsymbol{y})$ in the vicinity of the boundary Γ_m

The semi-infinite domains $G_1 =]-\infty, L_1[\times]0, l_2[\times]0, l_3[$ and $G_m =]0, \infty[\times]0, l_2[\times]\ 0, l_3[$, $m = 2,3$ are considered in the direction $\boldsymbol{e}_1$ normal, respectively to the faces Γ_1 and Γ_m, $m = 2,3$.

The boundary of G_1 at $(x_1 = L_1)$ and that of G_2, G_3 at $(x_1 = 0)$ are denoted $\Gamma'_m,\ m = 1,2,3$.

For $\boldsymbol{x} \in \Gamma_m$ and $\boldsymbol{y} = (y_1, y_2, y_3) \in G_m$, $m = 1,2,3$, the heterogeneous temperature field T^{ϵ} is searched under the asymptotic form: $T^{\epsilon}(\boldsymbol{x}) = T^{0}(\boldsymbol{x}) + (T^{1}(\boldsymbol{x},\boldsymbol{y}) + T_{BL}^{1,m}(\boldsymbol{x},\boldsymbol{y})) \in + \cdots$

The term $T_{BL}^{1,m}(\boldsymbol{x},\boldsymbol{y})$ is periodic in the $\{\boldsymbol{e}_2, \boldsymbol{e}_3\}$ directions.

Introducing the asymptotic expansion in the heat equation of the heterogeneous problem, and selecting the terms which have the same power ϵ^k, we get for $k = 0$

$$\mathrm{div}_y\left(\phi_{BL}^{0,m}(\boldsymbol{x},\boldsymbol{y})\right) = 0 \quad \text{in } G_m, \quad m = 1,2,3$$

with: $\phi_{BL}^{0,m}(\boldsymbol{x},\boldsymbol{y}) = K(y)\left(\nabla_y T_{BL}^{1,m}(\boldsymbol{x},\boldsymbol{y})\right)$

By introducing the functions $\boldsymbol{\chi^m}(\boldsymbol{y}) = \left[\chi_j^m(\boldsymbol{y})\right]_{j=1}^{3}$ in the above equation, such that:

$$T_{BL}^{1,m}(\boldsymbol{x},\boldsymbol{y}) = (\boldsymbol{\chi^m}(\boldsymbol{y}))^t.\nabla_{\boldsymbol{x}}\boldsymbol{T}^0(\boldsymbol{x})$$

It comes

$$div_y((\boldsymbol{K}(\boldsymbol{y})\nabla_{\boldsymbol{y}}\boldsymbol{\chi^m}(\boldsymbol{y}))\nabla_{\boldsymbol{x}}T^0(\boldsymbol{x})) = 0 \quad \text{in } G_m$$

$$\sum_{i=1}^{3}\frac{\partial T^0}{\partial x_i}(\boldsymbol{x})div_y(\boldsymbol{K}(\boldsymbol{y})\nabla_{\boldsymbol{y}}\chi_i^m(\boldsymbol{y})) = 0 \quad \text{in } G_m$$

which is satisfied if and only if:

$$div_y(\boldsymbol{K}(\boldsymbol{y})\nabla_{\boldsymbol{y}}\chi_i^{\boldsymbol{m}}(\boldsymbol{y})) = 0 \quad \text{in } G_m$$

This last equation will determine the functions $\left[\chi_j^m(y)\right]_{j=1}^{3}$ in the semi-infinite domain G_m, once boundary conditions will be set on Γ'_m.

A.1. The Dirichlet condition on Γ_1

For m = 1, we have: $T^{\epsilon}(s) = T_1 = 0$ *on* Γ_1

From the asymptotic expansion of T^{ϵ} in the vicinity of the boundary Γ_1, and by selecting the terms which have the same power ϵ^k, It comes, for $k = 0,1$:

$$T^0(x) = T_1 = 0; (T^1(\boldsymbol{x},\boldsymbol{y}) + T_{BL}^{1,1}(\boldsymbol{x},\boldsymbol{y})) = 0 \quad \text{on } \Gamma'_1$$

Using the properties of the solutions $T^1, T_{BL}^{1,1}$:

$$T^1(\boldsymbol{x},\boldsymbol{y}) = \sum_{i=1}^{3}\frac{\partial T^0}{\partial x_i}(\boldsymbol{x})w_i(\boldsymbol{y})$$

$$T_{BL}^{1,m=1}(\boldsymbol{x},\boldsymbol{y}) = \sum_{i=1}^{3}\frac{\partial T^0}{\partial x_i}(\boldsymbol{x}).\chi_i^{m=1}(\boldsymbol{y})$$

It comes:

$$\sum_{\mathrm{j}=1}^{3}\frac{\partial T^0}{\partial x_j}(x)(w_j(\boldsymbol{y}) + \boldsymbol{\chi}_j^{\boldsymbol{m}=1}(y)) = 0 \quad \text{on } \Gamma'_1$$

This equation is satisfied, if and only if:

$$w_j(y) + \chi_j^{m=1}(\boldsymbol{y}) = 0 \quad \text{on } \Gamma'_1$$

Which is the boundary condition on Γ'_1, to determine the functions $\left[\chi_j^{m=1}(y)\right]_{j=1}^{3}$

A.2. The Neumann boundary condition on Γ_2

For $m = 2$, we have: $\boldsymbol{\varphi}^{\epsilon}(s)\cdot n = \boldsymbol{K}(\boldsymbol{y})\nabla_{\boldsymbol{x}}T^{\epsilon}(x) = \varphi_2 \quad \text{on } \Gamma_2$.

By using the function derivation rule:

$$\nabla_{x,y}(T^1(x,y)) = \nabla_x T^1(x,y) + \frac{1}{\varepsilon}\nabla_y T^1(x,y)$$

And from the asymptotic expansion in the vicinity of the boundary Γ_2, by selecting the terms which have the same power ϵ^0, It comes

$$\left(\boldsymbol{K}(\boldsymbol{y})\left[\nabla_x T^0(\boldsymbol{x}) + \nabla_y T^1(\boldsymbol{x},\boldsymbol{y}) + \nabla_y T_{BL}^{1,2}(\boldsymbol{x},\boldsymbol{y})\right]\right)\cdot\boldsymbol{n} = \varphi_2 \quad \text{on } \Gamma_2'$$

Using the properties of the solutions $T^0, T^1, T_{BL}^{1,m}$:

$$T^0(\boldsymbol{x}) : \boldsymbol{K}_x^* T^0(\boldsymbol{x})\cdot\boldsymbol{n} = \varphi_2 \quad \text{on } \Gamma_2,$$

$$T^1(\boldsymbol{x},\boldsymbol{y}) = \sum_{i=1}^{3}\frac{\partial T^0}{\partial x_i}(\boldsymbol{x}).w_i(\boldsymbol{y})$$

$$T_{BL}^{1,m=2}(\boldsymbol{x},\boldsymbol{y}) = \sum_{i=1}^{3}\frac{\partial T^0}{\partial x_i}(\boldsymbol{x}).\chi_i^{m=2}(\boldsymbol{y})$$

Then: $\left(\boldsymbol{K}(\boldsymbol{y})\left[\nabla_x T^0(\boldsymbol{x}) + \nabla_y T^1(\boldsymbol{x},\boldsymbol{y}) + \nabla_y T_{BL}^{1,2}(\boldsymbol{x},\boldsymbol{y})\right]\right)\cdot\boldsymbol{n} = \boldsymbol{K}^*\nabla_x T^0(\boldsymbol{x})\cdot\boldsymbol{n}$ on Γ_2'

$$\boldsymbol{K}(\boldsymbol{y})\left[\sum_{j=1}^{3}\frac{\partial T^0}{\partial x_j}(\boldsymbol{x})e_j\right]\cdot\boldsymbol{n} + \boldsymbol{K}(\boldsymbol{y})\left[\sum_{j=1}^{3}\frac{\partial\, \mathrm{T}^0}{\partial x_j}(x)\nabla_y w_i(\boldsymbol{y})\right]\cdot\boldsymbol{n}$$
$$+\boldsymbol{K}(\boldsymbol{y})\left[\sum_{j=1}^{3}\frac{\partial T^0}{\partial x_j}(x)\right)\nabla_y\boldsymbol{\chi_j^m}(y)]\cdot\boldsymbol{n}$$
$$= \boldsymbol{K}^*\nabla_x T^0(\boldsymbol{x})\cdot\boldsymbol{n} \quad \text{on } \Gamma_2' \Rightarrow \sum_{j=1}^{3}\frac{\partial T^0}{\partial x_j}(\boldsymbol{x})\boldsymbol{K}(\boldsymbol{y})(\nabla_y\boldsymbol{\chi_j^m}(\boldsymbol{y}))\cdot\boldsymbol{n}$$
$$= -\sum_{j=1}^{3}\frac{\partial T^0}{\partial x_j}(\boldsymbol{x})\boldsymbol{K}(\boldsymbol{y})(\boldsymbol{e_j} + \nabla_y\boldsymbol{w_j}(\boldsymbol{y}))\cdot\boldsymbol{n} - \sum_{j=1}^{3}\frac{\partial T^0}{\partial x_j}(\boldsymbol{x})\boldsymbol{K}^*\boldsymbol{e_j}\cdot\boldsymbol{n}$$

This equation is satisfied if and only if:

$$K(y)(\nabla_y\boldsymbol{\chi_j^m}(y))\cdot\boldsymbol{n} = -\boldsymbol{K}(\boldsymbol{y})(\boldsymbol{e_j} + \nabla_y\boldsymbol{w_j}(\boldsymbol{y}))\cdot\boldsymbol{n} - \boldsymbol{K}^*\boldsymbol{e_j}\cdot\boldsymbol{n} \quad \text{on } \Gamma_2';\ j = 1,2,3$$

which is the boundary condition on Γ_2', to determine the functions $\left[\chi_j^{m=2}(y)\right]_{j=1}^{3}$

With $\boldsymbol{K}^*\boldsymbol{e_j} = \frac{1}{meas(Y)}\int_Y \boldsymbol{K}(\boldsymbol{y})(\boldsymbol{e_j} + \nabla_y w_j)dY,\ j = 1,..,3.$

A.3. The Fourier condition on Γ_3

For $m = 3$, we have: $\boldsymbol{\varphi}^{\epsilon}(s)\cdot\boldsymbol{n} = h\,(T^{\epsilon} - T_{ext})$ on Γ_3

From the asymptotic expansion of T^{ϵ} in the vicinity of the boundary Γ_3, and by selecting the terms which have the same power ϵ^0, it comes as above:

$$\left(\boldsymbol{K}(\boldsymbol{y})\left[\nabla_x T^0(\boldsymbol{x}) + \nabla_y T^1(\boldsymbol{x},\boldsymbol{y}) + \nabla_y T_{BL}^{1,3}(\boldsymbol{x},\boldsymbol{y})\right]\right)\cdot\boldsymbol{n}$$
$$= \gamma(T^0 - T_{ext}) \quad \text{on } \Gamma_3'$$

The solution $T^0(\boldsymbol{x})$ satisfies: $\boldsymbol{K}_x^* T^0(\boldsymbol{x})\cdot\boldsymbol{n} = h(T^0 - T_{ext})$ on Γ_3

Then by the same way that for the Neumann condition, we get the same boundary condition for the determination of the functions $\left[\chi_j^{m=3}(\boldsymbol{y})\right]_{j=1}^{3}$ on Γ_3':

$$\boldsymbol{K}(\boldsymbol{y})\left(\nabla_y\chi_j^{m=3}(\boldsymbol{y})\right)\cdot\boldsymbol{n} = -\boldsymbol{K}(\boldsymbol{y})(\boldsymbol{e_j} + \nabla_y\boldsymbol{w_j}(\boldsymbol{y})).\boldsymbol{n} - \boldsymbol{K}^*\boldsymbol{e_j}\cdot\boldsymbol{n} \quad \text{on } \Gamma_3';j = 1,2,3$$

The existence, the unicity and the behavior at infinity of the solution of this problem have been already studied in the literature [26]. Moreover, it is shown that the correcting terms $T_{BL}{}^{1,j}(x,y)$ are decreasing exponentially when $y1$ tends to ±infinity.

Appendix B. Eigenvalues Problem Statement for the determination of the depth of correcting terms $T_{BL}^{1,m}(\boldsymbol{x},\boldsymbol{y})$ in the vicinity of the boundary Γ_m

In both cases of Neumann and Fourier conditions, the functions $\chi_i^{m=2,3}(\boldsymbol{y})$ which determine the correcting terms $T_{BL}^{1,m}(\boldsymbol{x},\boldsymbol{y})$ on $G_m =]0,\infty[\ \times]0,l_2[\times]0,l_3[$, $m = 2,3$, are expressed under the form $\chi_i^m(\boldsymbol{y}) = \Psi_i^m(y)\cdot e^{-\delta_m y_1}$.

Starting with the equation: $\mathrm{div}_y(\boldsymbol{K}(\boldsymbol{y})(\nabla_{\boldsymbol{y}}\chi_i^m(\boldsymbol{y}))) = 0$ in G_m,

It implies: $\mathrm{div}_y(\boldsymbol{K}(\boldsymbol{y})(\nabla_y(\Psi_i^m(y).e^{-\delta_m y_1}))) = 0$ in G_m.

We have:

$$\nabla_y(\Psi_i^m(y).e^{-\delta_m y_1}) = \begin{bmatrix}\frac{\partial_i^m}{\partial y_1}e^{-\delta_m y_1} - \delta_m e^{-\delta_m y_1}\Psi_i^m\\ \frac{\partial_i^m}{\partial y_2}e^{-\delta_m y_1}\\ \frac{\partial_i^m}{\partial y_3}e^{-\delta_m y_1}\end{bmatrix} = e^{-\delta_m y_1}\begin{bmatrix}\frac{\partial_i^m}{\partial y_1} - \delta_m\Psi_i^m\\ \frac{\partial_i^m}{\partial y_2}\\ \frac{\partial_i^m}{\partial y_3}\end{bmatrix}$$

then:

$$\mathrm{div}_y(\boldsymbol{K}(\boldsymbol{y})(\nabla_y(\Psi_i^m(y).e^{-\delta_m y_1}))) = \mathrm{div}_y\left(e^{-\delta_m y_1}\boldsymbol{K}(\boldsymbol{y})\begin{bmatrix}\frac{\partial\Psi_i^m}{\partial y_1} - \delta_m\Psi_i^m\\ \frac{\partial\Psi_i^m}{\partial y_2}\\ \frac{\partial\Psi_i^m}{\partial y_3}\end{bmatrix}\right) = 0$$

which implies

$$e^{-\delta_m y_1}\left\{\mathrm{div}_y\left(\boldsymbol{K}(\boldsymbol{y})\begin{bmatrix}\frac{\partial\Psi_i^m}{\partial y_1} - \delta_m\Psi_i^m\\ \frac{\partial\Psi_i^m}{\partial y_2}\\ \frac{\partial\Psi_i^m}{\partial y_3}\end{bmatrix}\right) - \delta_m\left[\boldsymbol{k}_{11}\left(\frac{\partial\Psi_i^m}{\partial y_1} - \delta_m\Psi_i^m\right) + \boldsymbol{k}_{12}\frac{\partial_i^m}{\partial y_2} + \boldsymbol{k}_{13}\frac{\partial\Psi_i^m}{\partial y_3}\right]\right\} = 0$$

$$\mathrm{div}_y\left(\boldsymbol{K}(\boldsymbol{y})\begin{bmatrix}\frac{\partial\Psi_i^m}{\partial y_1} - \delta_m\Psi_i^m\\ \frac{\partial\Psi_i^m}{\partial y_2}\\ \frac{\partial\Psi_i^m}{\partial y_3}\end{bmatrix}\right) - \delta_m\left[\boldsymbol{k}_{11}\left(\frac{\partial\Psi_i^m}{\partial y_1} - \delta_m\Psi_i^m\right) + \boldsymbol{k}_{12}\frac{\partial\Psi_i^m}{\partial y_2} + \boldsymbol{k}_{13}\frac{\partial\Psi_i^m}{\partial y_3}\right] = 0$$

It follows that the parameter δ_m and the functions $\Psi_i^m(y)$ are the solutions of the eigenvalues problem:

$$\delta_m^2\boldsymbol{k}_{11}\Psi_i^m - \delta_m\left[\left(\frac{\partial k_{11}}{\partial y_1}\right) + \frac{\partial k_{12}}{\partial y_2} + \frac{\partial k_{13}}{\partial y_3}\right]\Psi_i^m + \mathrm{div}_y(\boldsymbol{K}\nabla_{\boldsymbol{y}}(\Psi_i^m))$$
$$-2\delta_m\begin{bmatrix}k_{11}\\ k_{12}\\ k_{13}\end{bmatrix}^t(\boldsymbol{K}\nabla_{\boldsymbol{y}}(\Psi_i^m)) = 0$$

References

[1] W.J. Parker, R.J. Jenkins, C.P. Butler, G. Abott, Flash method for determining thermal diffusivity, heat capacity and thermal conductivity, J. Appl. Phys. 32 (9) (1961) 1679–1684.

[2] P. Anderson, Thermal conductivity of some rubbers under pressure by the transient hot-wire method, J. Appl. Phys. 47 (6) (1976) 2424–2426.

[3] M. Thomas, N. Boyard, N. Lefevre, Y. Jarny, D. Delaunay, An experimental device for the simultaneous estimation of the thermal conductivity 3-D tensor and the specific heat of orthotropic composite materials, Compos. Sci. Technol. 53 (2010) 5487–5498.

[4] J. Jumel, D. Rochais, Measurement of thermal diffusivity, elastic anisotropy and crystallographic orientation by interferometric photothermal microscopy, J. Phys. D – Appl. Phys. 40 (13) (2007) 4060–4072.

[5] M. Quintard, S. Whitaker, One and two-equations models for transient diffusion process in two-phase systems, Adv. Heat Transfer 23 (1993) 3157–3169.

[6] G.C. Glatmaier, W.F. Ramirez, Use of volume averaging for the modeling of thermal properties of porous materials, Chem. Eng. Sci. 43 (12) (1988) 3157–3169.

[7] S. Whitaker, The Volume Averaging Method, Kluwer Academic Publishers., The Netherlands, 1999.

[8] A. Bensoussan, J.L. Lions, G. Papanicolaou, Asymptotic analysis for periodic structures, in: J.L. Lions, G. Papanicolaou, R.T. Rockafellar (Eds.), Studies in Mathematics and it is Applications, vol. 5, North Holland Ed., Amsterdam, 1978.

[9] J.L. Auriault, Effective macroscopic description for heat conduction in periodic composites, Int. J. Heat Mass Transfer 26 (6) (1983) 861–869.
[10] E. Sanchez-Palencia, Boundary layers and edge effects in composites, in: E. Sanchez-Palencia, A. Zaoui (Eds.), Homogenization Techniques for Composites Media, Lecture Notes in Physics, vol. 272, Springer-Verlag, Berlin, 1987, pp. 121–147.
[11] A. Dasgupta, R.K. Agarwal, Orthotropic thermal conductivity of plain-weave fabric composites using a homogenization technique, J. Comput. Math. 26 (18) (1992) 2736–2759.
[12] J. Auriault, C. Boutin, C. Geindreau, Homogenization of Coupled Phenomena in Heterogenous Media, John Wiley & Sons, 2010.
[13] M. Thomas, N. Boyard, L. Perez, Y. Jarny, D. Delaunay, Representative volume element of anisotropic unidirectional carbon–epoxy composite with high fiber volume fraction, Compos. Sci. Technol. 68 (2008) 3184–3192.
[14] M. Prat, Some refinements concerning the boundary conditions at the macroscopic level, Transp. Porous Med. 7 (2) (1992) 147–161.
[15] A. Degiovanni, Constriction impedance, Rev. Gen. Therm. 34 (406) (1995) 623–624.
[16] O. Fudym, J.C. Batsale, D. Lecomte, Heat diffusion at the boundary of stratified media homogenized temperature field and thermal constriction, Int. J. Heat Mass Transfer 47 (2004) 2437–2447.
[17] A. Bensoussan, J.L. Lions, G. Papanicolaou, Boundary layer analysis in homogenization of diffusion equations with Dirichlet conditions on the half space, in: K. Ito (Ed.), Proceedings of International Symposium on Stochastic Differential Equations, John Wiley & Sons, 1978, pp. 21–40.
[18] A. Bensoussan, J.L. Lions, G. Papanicolaou, Boundary layer analysis in homogenization of transport processes, Res. Inst. Math. Sci. 15 (1979) 53–157.
[19] H. Dumontet, Homogénéisation et effets de bord dans les matériaux composites –Doctoral thesis, Pierre et Marie Curie University, Paris, 1990.
[20] N. Buannic, P. Cartraud, Higher-order effective modeling of periodic heterogeneous beams Part 2: Derivation of the proper boundary conditions for the interior asymptotic solution, Int. J. Solids Struct. 38 (2001) 7163–7180.
[21] A.L. Kalamkarov, I.V. Andrianov, V.V. Danishevs'kyy, Asymptotic homogenization of composite materials and structures, Appl. Mech. Rev. 62 (2009) 030802.
[22] P. Kanouté, D.P. Boso, J.L. Chaboche, B.A. Schrefler, Multiscale methods for composites: a review, Arch. Comput. Methods Eng. 16 (1) (2009) 31–75.
[23] G. Panasenko, Multi-scale Modelling for Structures and Composites, Springer, 2005.
[24] F. Larsson, K. Runesson, F. Su, Variationally consistent computational homogenization of transient heat flow, Int. J. Numer. Methods Eng. 81 (2010) 1659–1686.
[25] M. Sahraoui, M. Kaviany, Slip and no-slip temperature boundary conditions at interface of porous, plain media: conduction, Int. J. Heat Mass Transfer 36 (1993) 1019–1033.
[26] J.A. Ochoa-Tapia, S. Whitaker, Heat transfer at the boundary between a porous medium and a homogeneous fluid, Int. J. Heat Mass Transfer 40 (11) (1997) 2691–2707.
[27] C.G. Aguilar-Madera, F.J. Valdés-Parada, B. Goyeau, J.A. Ochoa-Tapia, One-domain approach for heat transfer between a porous medium and a fluid, Int. J. Heat Mass Transfer 54 (2011) 2089–2099.
[28] M. Chandesris, D. Jamet, Boundary conditions at a planar fluid–porous interface for a Poiseuille flow, Int. J. Heat Mass Transfer 49 (2006) 2137–2150.
[29] G. Allaire, M. Amar, Boundary layer tails in periodic homogenization, ESAIM: Control Optim. Calculus Variations 4 (1999) 209–243.
[30] M. Amar, M. Tarallo, S. Terracini, On the exponential decay for boundary layer problems, C. R. Acad. Sci. Paris 328 (1) (1999) 1139–1144.
[31] A. Matine, N. Boyard, Y. Jarny, G. Legrain, P. Cartraud, M. Thomas, Effective thermal conductivity tensor of composite materials: Determination of the representative volume element, in: Sixth International Conference on Inverse Problem: Identification, Design and Control, 10th–12th October, Moscow, Russia, 2010.